Magnetic circular dichroism and absorption spectrum of zinc phthalocyanine in an argon matrix between 14700 and 74000 cm−1

ARTICLE *in* THE JOURNAL OF PHYSICAL CHEMISTRY · APRIL 1989

Impact Factor: 2.78 · DOI: 10.1021/j100345a028

7 AUTHORS, INCLUDING:

Bryce Williamson
University of Canterbury
57 PUBLICATIONS **653** CITATIONS
SEE PROFILE

Andreas Schrimpf
Philipps University of Marburg
21 PUBLICATIONS **168** CITATIONS
SEE PROFILE

functional approximation used in the computations. There are very few computations for arene–metal complexes that are of sufficient quality to predict their bond and total energies accurately. In order to determine whether the LCAO–LSD method can generally predict these properties, more computations on a whole series of arene–metal compounds must be performed and compared with accurate experimental data.

Acknowledgment. Saba M. Mattar acknowledges the financial assistance from the Natural Science and Engineering Research Council of Canada, the University of New Brunswick Research Fund, and the allocation of computer time from the Computer Center of the University of New Brunswick.

Registry No. $(\eta^6\text{-}C_6H_6)V$, 61332-91-0; $(\eta^6\text{-}C_6H_6)V^+$, 102307-49-3.

Magnetic Circular Dichroism and Absorption Spectrum of Zinc Phthalocyanine in an Argon Matrix between 14 700 and 74 000 cm^{-1}

Thomas C. VanCott,[†] Janna L. Rose,[†] G. Christian Misener,[†,§] Bryce E. Williamson,*[,‡] Andreas E. Schrimpf,[†,∥] Michael E. Boyle,[†,⊥] and Paul N. Schatz*[,†]

The Chemistry Department, University of Virginia, Charlottesville, Virginia 22901, and The Chemistry Department, University of Canterbury, Christchurch 1, New Zealand *(Received: July 14, 1988; In Final Form: September 26, 1988)*

The magnetic circular dichroism (MCD) and absorption spectra of zinc phthalocyanine (ZnPc) isolated in an Ar matrix have been studied over the range 14 700–74 000 cm^{-1}. Synchrotron radiation, from the electron storage ring at the Synchrotron Radiation Center, Madison, WI, was used for energies above 33 000 cm^{-1}. The spectra are well resolved, and the MCD permits the determination of excited-state magnetic moments. There is strong evidence that the Pc rings are preferentially oriented with the molecular planes parallel to the deposition window. The data can be reasonably correlated with the old Peel calculation of Henriksson et al., but there is a compelling need for a new calculation that extends to higher energy and includes extensive configuration interaction.

I. Introduction

The phthalocyanines (Pc) are molecules with many interesting and useful properties. Nyokong et al.[1] have recently summarized some of these properties and given a review of the relevant spectroscopic literature. A comprehensive review can also be found in the dissertation of Misener.[2]

Despite considerable work, the ultraviolet (UV) and vacuum ultraviolet spectra of Pc's remain poorly understood. To assign such spectra with confidence, it is necessary to have a clear knowledge of the total number of transitions as well as the energy and excited-state symmetry of each individual transition, information that would normally require sharp-band spectra of oriented samples. Most spectra of Pc's that have been reported previously are of randomly oriented samples and show broad bands. Bajema et al.,[3] Bondybey and English,[4] and Huang et al.[5,6] have demonstrated that very much sharper spectra can be obtained from dilute matrices at low temperatures. The later workers,[4-6] using selective excitation techniques, were able to resolve extensive vibronic structure association with the lowest energy $\pi \rightarrow \pi^*$ transition.

Nyokong et al.[1] recently presented a detailed spectral analysis, over the region ~11 600–43 000 cm^{-1}, of ZnPc(L) and the π-cation-radical species, $ZnPc(L)^+$, in solution, where L is an axially coordinated cyanide, imidazole, or pyridine ligand. To determine the excited-state symmetries, they measured the magnetic circular dichroism (MCD) as well as the absorption spectra; the presence of $\mathcal{A}$-terms in the MCD is a clear indication of excited-state degeneracy.[7] These workers suggested assignments on the basis of extensive band envelope deconvolution of the absorption and MCD spectra. (We compare our results with those of Nyokong et al. in section VII.)

In this work we report the MCD and absorption spectra of ZnPc in an argon matrix (ZnPc/Ar) at ~5 K. This approach combines the advantage of MCD in determining excited-state symmetries with the sharper bands that are a consequence of low temperature and isolation of the chromophore in an "inert" medium. It has the additional advantage that the host material remains transparent well into the vacuum-UV so that the range of investigation is not restricted by solvent absorption. As an unexpected bonus, we have found considerable evidence that the guest molecules assume a preferred orientation in the matrix, which allows the extraction of additional information concerning the excited-state symmetries.

ZnPc is well suited for a study that emphasizes the spectroscopy of the Pc^{2-} ligand. The central Zn^{2+} ion has a d^{10} configuration, so ligand-to-metal charge-transfer and d–d transitions should not complicate the spectra. The crystal structure of β-ZnPc shows the molecules to be centrosymmetric and, geometrically, almost within experimental error of D_{4h} symmetry.[8] Deviations from 4-fold symmetry are important to a detailed analysis of the MCD, since molecules with 2-fold or lower symmetry can have no degenerate states and thus cannot show "true" $\mathcal{A}$ terms.[7] However, if the deviations are small, it remains a useful and valid ap-

[†] University of Virginia.
[‡] University of Canterbury.
[§] Present address: Environmental Technologies Group, 1400 Taylor Ave., PO Box 9840, Baltimore, MD 21284.
[⊥] Present address: Code 6123, Naval Research Laboratory, Washington, D.C. 20375-5000.
[∥] Present address: Fachbereich Physik der Philipps Universität, Marburg, Federal Republic of Germany.

(1) Nyokong, T.; Gasyna, Z.; Stillman, M. J. *Inorg. Chem.* **1987**, *26*, 1087–1095, and references therein.
(2) Misener, G. C. Ph.D. Thesis, University of Virginia, Charlottesville, VA, 1987, and references therein.
(3) Bajema, L.; Gouterman, M.; Meyer, B. *J. Mol. Spectrosc.* **1968**, *27*, 225–235.
(4) Bondybey, V. E.; English, J. H. *J. Am. Chem. Soc.* **1979**, *101*, 3446–3450.
(5) Huang, T. H.; Reickhoff, K. E.; Voigt, E. M. *J. Chem. Phys.* **1982**, *77*, 3424–3441.
(6) Huang, T. H.; Rieckhoff, K. E.; Voigt, E. M. *J. Phys. Chem.* **1981**, *85*, 3322–3326.
(7) Piepho, S. B.; Schatz, P. N. *Group Theory in Spectroscopy with Applications to Magnetic Circular Dichroism*; Wiley: New York, 1983.
(8) Scheidt, W. R.; Dow, W. *J. Am. Chem. Soc.* **1977**, *99*, 1101–1104.

0022-3654/89/2093-2999$01.50/0

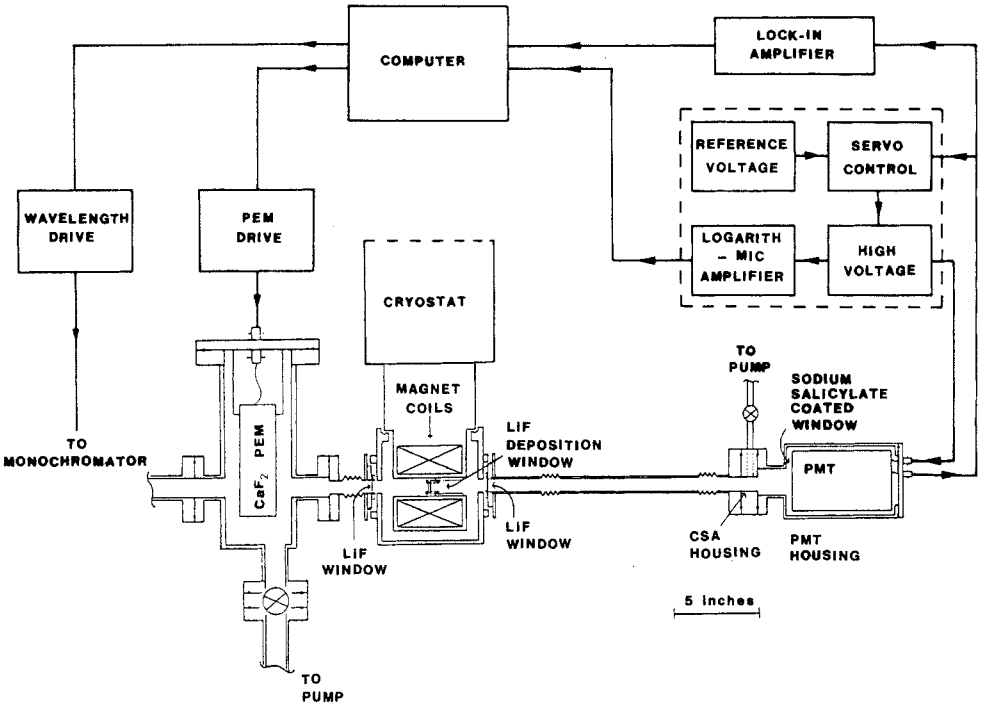

Figure 1. Equipment for the measurement of MCD and single-beam absorbance of matrix isolated samples in the vacuum-UV. PEM = photoelastic modulator, PMT = photomultiplier tube, CSA = *d*-10-camphorsulfonic acid. See text for explanation.

proximation to formally regard the molecules as having the higher symmetry. In this paper we generally treat the molecule as having D_{4h} symmetry but draw attention to specific evidence of lower symmetry in at least some of the excited states.

Angular momentum information obtained from the MCD provides a useful test of the excited-state wave functions determined by molecular orbital methods. Despite the fact that the treatment of Henriksson, Roos, and Sundbom[9] (HRS) was performed some 15 years ago, it still seems the most useful one for comparison with the spectra of Pc's over a wide energy range. In section VI we compare our results with the calculations of HRS.

II. Experimental Section

ZnPc was provided by Professor Martin J. Stillman of the University of Western Ontario. Samples were sublimed from a quartz Knudsen cell at ~380 °C and codeposited with a large excess of Ar gas on a cryogenically cooled LiF window in the bore of a superconducting solenoid. The tail of the cryostat, containing the magnet and deposition window, was then rotated by 90° into the optical path.

It became clear in the present work, as we discuss later, that some of the spectral features reported in an earlier note[10] are attributable to phthalonitrile (Pn; 1,2-dicyanobenzene) and in one case to Zn atoms, starting materials in the preparation of ZnPc. Although pure samples of Pn are found to be readily sublimed at 85 °C,[11] heating a sample of ZnPc overnight at 300 °C under vacuum does not remove this impurity, which is evidently occluded in the ZnPc crystal. ZnPc/Ar matrices free from Pn were eventually produced by using the portion of a ZnPc sample remaining after the Pn spectral bands ceased to grow during a preliminary deposition using a closed-cycle helium regrigerator. The $^1S \rightarrow {}^1P$ band of Zn, at 48 200 cm^{-1}, was removed here by subtracting the spectra obtained for pure Zn in an Ar matrix.

Spectra were measured at a temperature of ~5 K and at field strengths between 0.36 T (for the sharp Q(0,0) structure) and 3.75 T (for the broader UV bands). Some absorption measurements were made with the sample rotated by up to 30° about the vertical axis to check for preferential molecular orientation within the sample (section IV.2).

The data between 14 700 and 33 000 cm^{-1} were recorded at the University of Virginia by using a spectrometer that permits simultaneous recording of the MCD and double-beam absorption spectra. The principles of this spectrometer have been outlined previously[12] and are discussed in detail in the dissertation of Misener.[2] The data between 33 000 and 74 000 cm^{-1} were collected at the Synchrotron Radiation Center of the University of Wisconsin—Madison, by using a 1-GeV electron storage ring (Aladdin) and either a 4-m normal incidence monochromator or a 1-m Al Seya-Namioka monochromator.

A schematic depiction of the vacuum-UV apparatus is shown in Figure 1. Linearly polarized synchrotron radiation from the monochromator is modulated between right-hand and left-hand circular polarization at 50 kHz by a CaF_2 photoelastic modulator. It then passes through the magnet bore and the sample to the photomultiplier tube (PMT), the front window of which is coated with a sodium salicylate scintillator. A servo circuit adjusts the PMT high voltage to maintain a constant dc output signal. A signal proportional to the high voltage is amplified logarithmically to give the single-beam absorbance, and the 50-kHz component of the signal, which is proportional to the MCD, is measured by a lock-in amplifier. Further details of the vacuum-UV instrumentation may be found elsewhere.[13]

The absorption base line prior to deposition and the (zero-field) MCD base line after deposition were subtracted from the absorption and MCD signals, respectively. Spectra were calibrated against the absorbance and natural CD of standard solutions of *d*-10-camphorsulfonic acid (vacuum-UV) or Λ-tris(1,2-ethanediamine)cobalt(III) (visible and near-UV). Depolarization due to the matrices, as measured by comparing the CD of the standard solutions inserted after the sample with the CD of the standards in the absence of the sample, was found to be negligible.

III. Results

In Figure 2, the absorption spectrum of ZnPc/Ar over the range 14 300–74 000 cm^{-1} is compared with the gas-phase[14] and thin-

(9) Henriksson, A.; Roos, B.; Sundbom, M. *Theoret. Chim. Acta* **1972**, *27*, 303–313.
(10) Williamson, B. E.; Boyle, M. E.; Schatz, P. N.; Marks, J. P.; Snyder, P. A. *Chem. Phys. Lett.* **1987**, *140*, 483–488.
(11) Rose, J. L.; Van Cott, T. C.; Schrimpf, A. E.; Williamson, B. E.; Schatz, P. N., manuscript in preparation.
(12) Rose, J.; Smith, D.; Williamson, B. E.; Schatz, P. N.; O'Brien, M. C. M. *J. Phys. Chem.* **1986**, *90*, 2608–2615.
(13) Boyle, M. E. Ph.D. Thesis, University of Virginia, Charlottesville, VA, 1987.
(14) Edwards, L.; Gouterman, M. *J. Mol. Spectrosc.* **1970**, *33*, 292–310.

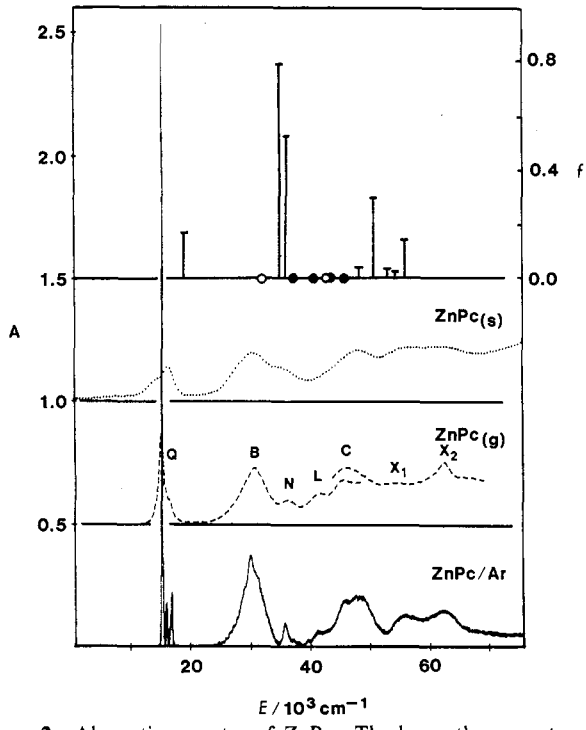

Figure 2. Absorption spectra of ZnPc. The lower three spectra are (bottom to top) ZnPc/Ar at ~5 K, gas-phase ZnPc at ~800 K from ref 14, and thin-film ZnPc from ref 15. The labels Q, B, N, L, C, X_1, and X_2 for the gas-phase data follow the notation of ref 14. The absorbance scale (left-hand side) pertains to the ZnPc/Ar spectrum below 33 000 cm^{-1}. The ZnPc/Ar spectrum above 33 000 cm^{-1} was obtained with synchrotron radiation and is normalized to the same absorbance scale. The gas-phase and thin-film data are normalized to give the same integrated intensity in the Q-band region as the matrix data. The calculated spectrum of ref 9 is shown at the top of the figure, with the oscillator strength (f) on the right-hand side. Open circles indicate z-polarized ($n \rightarrow \pi^*$) transitions, and solid circles indicate x,y-polarized ($\pi \rightarrow \pi^*$) transitions with oscillator strengths less than 0.01.

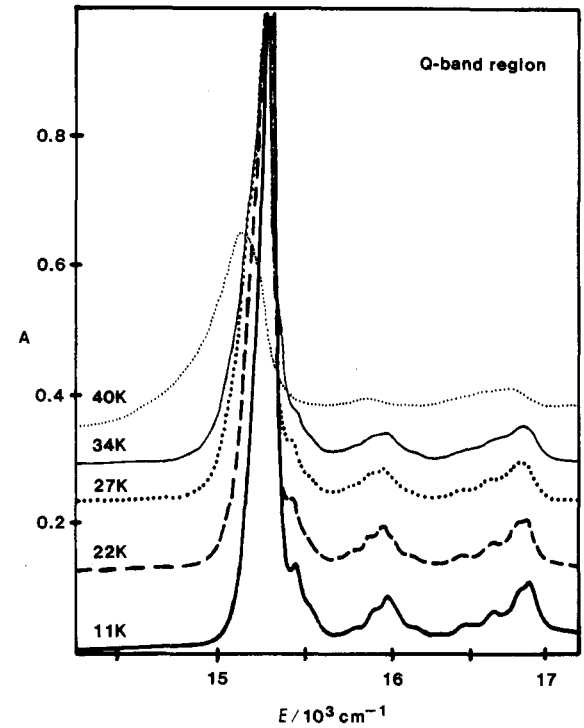

Figure 3. Effect of annealing on the Q-band region of the ZnPc/Ar absorption spectrum. A matrix deposited at ~11 K gave the spectrum shown at the bottom of the figure. After annealing by warming the matrix to the temperatures indicated on the left-hand side and recooling to 11 K, the band envelopes become progressively broader and shift to lower energy (see section III).

film[15] absorption spectra of ZnPc. Correlations between the three sets of absorption data are clearly evident. We therefore retain the notation of Edwards and Gouterman,[14] Q, B, N, L, X_1, and X_2, but refer it to spectral regions rather than to individual bands. The spectra have been normalized so that the integrated intensity in the Q-band region is the same for all three cases. The MCD and more detailed absorption spectra of ZnPc/Ar in each region are reproduced in Figures 5–10.

The matrix spectra, as expected, show sharper bands and much more structure than the gas-phase, thin-film, or solution spectra. This is most clearly illustrated in the Q-band region (10 000–20 000 cm^{-1}, Figures 2 and 5–7). For example, the Q(0,0) absorption envelope of a matrix obtained at a deposition temperature of ~5 K (Figure 5), includes at least 12 peaks and shoulders, each of which is associated with a maximum or a minimum in the MCD. Similar absorption spectra were observed by Bajema et al. for ZnPc in noble-gas matrices,[3] but their ZnPc/Ar spectrum differs from ours in the detail of the fine structure.

We have found that the fine structure of the ZnPc/Ar spectra is dependent on the conditions under which the matrix is formed and can be modified by annealing the matrix. For example, the absorption spectrum of the Q-band region of a matrix obtained with a deposition temperature of ~11 K is shown in the lowest spectrum of Figure 3. After annealing of the matrix, by warming to temperatures as high as ~40 K and recooling to 11 K (upper curves, Figure 3), the absorption bands become progressively broader and shift to the red. Similar behavior is observed in other regions but is less pronounced due to the presence of broader bands. Our interpretation of this behavior is that ZnPc molecules reside at several inequivalent sites within the matrix. In matrices deposited at the lower temperatures, the positions of the nearest-neighbor host atoms are determined largely by the structure of the MPc molecule. The thermal energy is insufficient for these atoms to relax into positions commensurate with the bulk Ar lattice, and several well-defined, discrete impurity sites results. On annealing, the structure around the impurity assimilates with the structure of the bulk lattice, resulting in a large number of sites, which vary from each other in a quasi-continuous manner. The discrete sites result in sharp-band spectra, and the quasi-continuous sites result in broad-band spectra.

Absorption spectra obtained with the deposition window rotated about the vertical by ~30° vary somewhat from one matrix to another. They are very similar to those obtained with the window perpendicular to the optical axis but generally show an overall decrease in absorbance. The only consistent exception to this is a band at 32 200 cm^{-1}, on the blue edge of the B-band region, which shows a substantial increase in absorbance for *all* matrices. A particularly clear illustration of this is given in Figure 4. The presence of two types of dependence on the angle of rotation for each sample suggests that the ZnPc molecules are preferentially oriented within the matrix (section IV.2). The general decrease in absorbance observed in most cases is attributed to inhomogeneity of the matrices.

IV. Theoretical Aspects of Data Analysis

Assuming D_{4h} symmetry, the ground-state of ZnPc is $^1A_{1g}$ and only $\mathcal{A}$ terms and $\mathcal{B}$ terms can contribute to the MCD.[7] If the symmetry is lower but approximates D_{4h}, the $\mathcal{A}$ terms are replaced by pseudo-$\mathcal{A}$ terms. The theoretical treatment, however, remains identical,[7] and for that reason we treat the case for full D_{4h} symmetry in this section. We assume that only the zero-point vibrational level of the ground state is populated at ~5 K and that spin–orbit effects are unimportant since Zn^{2+} has a d^{10} configuration.

1. Fully Allowed Transitions. Calculation of MCD Parameters. π-Orbitals of the Pc ligand transform antisymmetrically with respect to σ_h (reflection in the plane of the molecule), and inspection of the D_{4h} character table shows that they must belong to the irreps (irreducible representations) γ_u or e_g, where γ is used throughout to represent a_1, a_2, b_1, or b_2. Conversely, σ-orbitals

(15) Schechtman, B. H.; Spicer, W. E. *J. Mol. Spectrosc.* **1970**, *33*, 28–48.

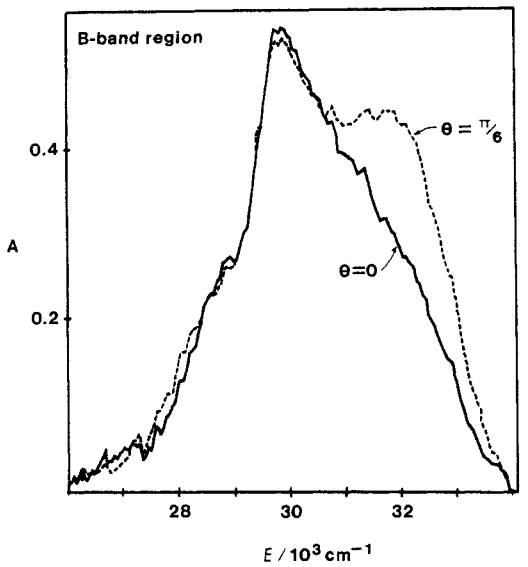

Figure 4. Orientation dependence of the ZnPc/Ar absorption spectrum in the B-band region. The full curve was obtained with the deposition window perpendicular to the optical axis, while the dashed curve was obtained with the window rotated by 30° about the vertical. The additional intensity centered near 32 200 cm^{-1} in the dashed spectrum gives evidence of strong preferential orientation of the ZnPc molecules and the presence of a z-polarized ($n \rightarrow \pi^*$) transition (see section IV.2).

transform symmetrically with respect to σ_h and belong to the irreps γ_g or e_u. The relative positions of the higher lying occupied and lower lying unoccupied MOs, determined by Henrikson, Roos, and Sundbom[9] (HRS), are shown in Figure 11. The orbitals closest to the HOMO–LUMO gap are π-orbitals, while the σ-orbitals $1b_{2g}$, $2e_u$, and $2a_{1g}$ are nonbonding, lone-pair orbitals of the bridging nitrogen atoms, $n(N_{p_\sigma})$. In the spectral region investigated we would expect to observe transitions arising from $\pi \rightarrow \pi^*$ and $n(N_{p_\sigma}) \rightarrow \pi^*$ excitations.

The only fully allowed electric dipole transitions for ZnPc are $^1A_{1g} \rightarrow {}^1E_u$ and $^1A_{1g} \rightarrow {}^1A_{2u}$. The former are polarized within the plane of the molecule (x,y-polarized), can give rise to both $\mathcal{A}$ terms and $\mathcal{B}$ terms in the MCD, and must arise from $\pi \rightarrow \pi^*$ (or $\sigma \rightarrow \sigma^*$) excitations. The latter are z-polarized, can give rise to $\mathcal{B}$ terms only, and must arise from $\sigma \rightarrow \pi^*$ (or $\pi \rightarrow \sigma^*$) excitations. Thus in particular, any allowed transition arising from $\pi \rightarrow \pi^*$ excitations must show an $\mathcal{A}$ term unless the excited-state angular momentum is accidentally small or a $\mathcal{B}$ term is overwhelmingly dominant.

For a fully allowed electronic transition between Born–Oppenheimer states in the rigid shift approximation, the MCD (ΔA) and absorbance (A) are given by[7]

$$\Delta A/\mathcal{E} = 152.5Bcl[\mathcal{A}_1(-df(\mathcal{E})/d\mathcal{E}) + (\mathcal{B}_0 + \mathcal{C}_0/kT)f(\mathcal{E})] \quad (1)$$

$$A/\mathcal{E} = 326.6cl\mathcal{D}_0 f(\mathcal{E}) \quad (2)$$

$\mathcal{E} = h\nu$ is the photon energy (in cm^{-1}), B is the magnetic induction in tesla, cl is the product of the concentration and path length of the sample in mmol cm^{-2}, and $f(\mathcal{E})$ is a normalized band-shape function.

For well-separated transitions, ratios of the MCD (per tesla) and absorption parameters can be obtained by direct integration of the experimental data, without explicit knowledge of the function $f(\mathcal{E})$ or the quantity cl. For ZnPc the appropriate equations are[7]

$$\frac{\mathcal{A}_1}{\mathcal{D}_0} = 2.142\frac{\int(\Delta A/\mathcal{E})(\mathcal{E} - \bar{\mathcal{E}})\,d\mathcal{E}}{\int(A/\mathcal{E})\,d\mathcal{E}} \quad (3a)$$

$$\frac{\mathcal{B}_0}{\mathcal{D}_0} = 2.142\frac{\int(\Delta A/\mathcal{E})\,d\mathcal{E}}{\int(A/\mathcal{E})\,d\mathcal{E}} \quad (3b)$$

$$\mathcal{C}_0/\mathcal{D}_0 = 0 \quad (3c)$$

where $\bar{\mathcal{E}}$ is the band barycenter, defined by

$$\bar{\mathcal{E}} = \frac{\int A\,d\mathcal{E}}{\int(A/\mathcal{E})\,d\mathcal{E}} \quad (4)$$

Equations 3b and 3c are obtained by using the fact that ZnPc has a nondegenerate ground state and therefore $\mathcal{C}_0 = 0$.[7]

If we assume random molecular orientation, the theoretical expressions for an allowed transition, $^1A_{1g} \rightarrow J$, in the absence of spin–orbit coupling, are

$$\bar{\mathcal{A}}_1(J) = (i/3)\sum_{\lambda\lambda'}\langle J\lambda|\mathbf{L}|J\lambda'\rangle\cdot\langle {}^1A_{1g}|\mathbf{m}|J\lambda\rangle\mathbf{x}\langle J\lambda'|\mathbf{m}|{}^1A_{1g}\rangle \quad (5a)$$

$$\bar{\mathcal{B}}_0(J) = \frac{2}{3}\,\mathrm{Im}\left\{\sum_{\lambda}\sum_{\substack{K\kappa \\ (K\neq J)}}\frac{\langle J\lambda|\mathbf{L}|K\kappa\rangle}{E_K - E_J}\right\}\cdot\langle {}^1A_{1g}|\mathbf{m}|J\lambda\rangle\mathbf{x}\langle K\kappa|\mathbf{m}|{}^1A_{1g}\rangle \quad (5b)$$

$$\bar{\mathcal{D}}_0(J) = \tfrac{1}{3}\sum_{\lambda}|\langle {}^1A_{1g}|\mathbf{m}|J\lambda\rangle|^2 \quad (5c)$$

In these equations the parameters on the left-hand side are space averaged, and all matrix elements pertain to zero-field states in their equilibrium nuclear configurations. E_J and λ are the energy and partner label, respectively, of the final state, J, while E_K and κ are the corresponding quantities for the state K. Im indicates the imaginary part of a complex function, and $i = (-1)^{1/2}$. The electric dipole operator, $\mathbf{m}$, and the orbital angular momentum operator, $\mathbf{L}$, are fixed in the molecular reference frame (denoted hereafter by lower case x,y,z). Equation 5b is obtained by assuming that the ground state ($^1A_{1g}$) is well separated from all other states, so that field-induced mixing only between excited states need be considered.

For $^1A_{1g} \rightarrow {}^1E_u^a$ one obtains

$$\bar{\mathcal{A}}_1({}^1E_u^a) = \frac{2i}{3}\langle {}^1E_u^a x|L_z|{}^1E_u^a y\rangle|\langle {}^1A_{1g}|m_x|{}^1E_u^a x\rangle|^2 \quad (6a)$$

$$\bar{\mathcal{B}}_0({}^1E_u^a) = \bar{\mathcal{B}}_0({}^1E_u^a, {}^1E_u^n) + \bar{\mathcal{B}}_0({}^1E_u^a, {}^1A_{2u}^n) \quad (6b)$$

$$\bar{\mathcal{B}}_0({}^1E_u^a, {}^1E_u^n) = \frac{4}{3}\,\mathrm{Im}\left\{\sum_{n\neq a}\frac{\langle {}^1E_u^a x|L_z|{}^1E_u^n y\rangle\langle {}^1A_{1g}|m_x|{}^1E_u^a x\rangle\langle {}^1E_u^n y|m_y|{}^1A_{1g}\rangle}{E_n - E_a}\right\} \quad (6c)$$

$$\bar{\mathcal{B}}_0({}^1E_u^a, {}^1A_{2u}^n) = \frac{-4}{3}\,\mathrm{Im}\left\{\sum_{n}\frac{\langle {}^1E_u^a x|L_y|{}^1A_{2u}^n\rangle\langle {}^1A_{1g}|m_x|{}^1E_u^a x\rangle\langle {}^1A_{2u}|m_z|{}^1A_{1g}\rangle}{E_n - E_a}\right\} \quad (6d)$$

$$\bar{\mathcal{D}}_0({}^1E_u^a) = \tfrac{2}{3}|\langle {}^1A_{1g}|m_x|{}^1E_u^a x\rangle|^2 \quad (6e)$$

Equations 6a–e are expressed in molecular-fixed Cartesian basis sets. L_η transforms as the rotational operator R_η ($\eta = x$, y, or z) and $|E_u x\rangle$, $|E_u y\rangle$, and $|A_{2u}\rangle$ transform respectively like x, y, and z.

For $^1A_{1g} \rightarrow {}^1A_{2u}^a$ the corresponding expressions are

$$\bar{\mathcal{A}}_1({}^1A_{2u}^a) = 0 \quad (7a)$$

$$\bar{\mathcal{B}}_0({}^1A_{2u}^a) = \frac{4}{3}\,\mathrm{Im}\left\{\sum_{n}\frac{\langle {}^1A_{2u}^a|L_y|{}^1E_u^n x\rangle\langle {}^1A_{1g}|m_z|{}^1A_{2u}^a\rangle\langle {}^1E_u^n x|m_x|{}^1A_{1g}\rangle}{E_n - E_a}\right\} \quad (7b)$$

$$\bar{\mathcal{D}}_0({}^1A_{2u}^a) = \tfrac{1}{3}|\langle {}^1A_{1g}|m_z|{}^1A_{2u}^a\rangle|^2 \quad (7c)$$

2. Molecular Orientation. There is considerable reason to believe that large planar molecules such as ZnPc assume a preferential orientation with the molecular x,y plane parallel to the deposition window.[16] In that case the treatment leading to eq 5 must be modified since orientational averaging now applies only in the space-fixed X,Y plane. (The direction of both the

magnetic field and the optical path is denoted Z in the space-fixed X,Y,Z reference frame). If preferential orientation is complete, the results are

$$\mathcal{A}_1^z(J) = i\sum_{\lambda\lambda'}\langle J\lambda|L_z|J\lambda'\rangle \mathbf{k}\cdot\langle {}^1A_{1g}|\mathbf{m}|J\lambda\rangle \mathbf{x}\langle J\lambda'|\mathbf{m}|{}^1A_{1g}\rangle \quad (8a)$$

$$\mathcal{B}_0^z(J) = 2\ \mathrm{Im}\left\{\sum_{\lambda}\sum_{\substack{K\kappa\\(K\neq J)}}\frac{\langle J\lambda|L_z|K\kappa\rangle}{E_K - E_J}\mathbf{k}\cdot\langle {}^1A_{1g}|\mathbf{m}|J\lambda\rangle \mathbf{x}\langle K\kappa|\mathbf{m}|{}^1A_{1g}\rangle\right\} \quad (8b)$$

$$\mathcal{D}_0^z(J) = \tfrac{1}{2}\sum_{\lambda}(|\langle {}^1A_{1g}|m_x|J\lambda\rangle|^2 + |\langle {}^1A_{1g}|m_y|J\lambda\rangle|^2) \quad (8c)$$

The superscripts z on the left-hand side of eq 8 indicate that these parameters apply to the case where the molecular z axis is parallel with the optical Z axis. $\mathbf{k}$ is a unit vector in the z direction.

For ${}^1A_{1g} \rightarrow {}^1E_u^a$ one immediately finds

$$\mathcal{A}_1^z({}^1E_u^a) = 3\bar{\mathcal{A}}_1({}^1E_u^a) \quad (9a)$$

$$\mathcal{B}_0^z({}^1E_u^a) = 3\bar{\mathcal{B}}_0({}^1E_u^a, {}^1E_u^n) \quad (9b)$$

$$\mathcal{D}_0^z({}^1E_u^a) = \tfrac{3}{2}\bar{\mathcal{D}}_0({}^1E_u^a) \quad (9c)$$

where the parameters on the right-hand side are given by eq 6. For ${}^1A_{1g} \rightarrow {}^1A_{2u}^a$

$$\mathcal{A}_1^z({}^1A_{2u}^a) = \mathcal{B}_0^z({}^1A_{2u}^a) = \mathcal{D}_0^z({}^1A_{2u}^a) = 0 \quad (10)$$

The important point about eq 9 and 10 is that the experimentally measurable quantities are dependent on the degree of preferential orientation. In the case where molecular orientation is complete and the deposition window is perpendicular to Z, no absorption will be observed for allowed $\sigma \rightarrow \pi^*$ (or $\pi \rightarrow \sigma^*$) transitions, while for a $\pi \rightarrow \pi^*$ (or $\sigma \rightarrow \sigma^*$) transition (${}^1A_{1g} \rightarrow {}^1E_u^a$)

$$\frac{\mathcal{A}_1^z({}^1E_u^a)}{\mathcal{D}_0^z({}^1E_u^a)} = \frac{2\bar{\mathcal{A}}_1({}^1E_u^a)}{\bar{\mathcal{D}}_0({}^1E_u^a)} \quad (11a)$$

$$\frac{\mathcal{B}_0^z({}^1E_u^a)}{\mathcal{D}_0^z({}^1E_u^a)} = \frac{2\bar{\mathcal{B}}_0({}^1E_u^a, {}^1E_u^n)}{\bar{\mathcal{D}}_0({}^1E_u^a)} \quad (11b)$$

The existence of complete (or near complete) molecular orientation can, in principle, be tested by monitoring the dependence of the absorption intensity on rotation of the deposition window about the vertical (X) axis.

For the randomly oriented case we would predict, for a perfectly homogeneous matrix

$$\bar{A}_\theta(J) = \bar{A}_0(J)/\cos\alpha \quad (12a)$$

where

$$\alpha = \sin^{-1}\left(\frac{\sin\theta}{n_{Ar}}\right) \quad (12b)$$

$\bar{A}_\theta(J)$ is the absorbance corresponding to the transition ${}^1A_{1g} \rightarrow J$ that would be observed when the matrix is rotated by θ about X and the bars indicate that the absorbance values pertain to the randomly oriented case. The factor $1/\cos\alpha$ accounts for the change in path length; α is the effective rotational angle allowing for the refractive index of solid argon ($n_{Ar} = 1.29$). Under these conditions we would expect the apparent absorbance of *all* transitions to increase by ~8% between $\theta = 0$ and $\theta = \pi/6$.

For the case of complete preferential orientation, again assuming perfect homogeneity

$$A_\theta^z({}^1E_u) = A_0^z({}^1E_u)\frac{1 + \cos^2\alpha}{2\cos\alpha} \quad (13a)$$

$$A_\theta^z({}^1A_{2u}) = A_0^x({}^1A_{2u})\frac{\sin^2\alpha}{\cos\alpha} \quad (13b)$$

where $A_\theta^\eta(J)$ is the absorbance corresponding to ${}^1A_{1g} \rightarrow J$ that would be observed in the case where all molecules are oriented with their η axes ($\eta = x$ or z) perpendicular to the deposition window, and the window is rotated by θ about X. Here we would expect two types of dependence on θ. ${}^1A_{1g} \rightarrow {}^1E_u$ bands should increase in absorbance by only ~0.3% between $\theta = 0$ and $\theta = \pi/6$, whereas ${}^1A_{1g} \rightarrow {}^1A_{2u}$ bands should increase from zero absorbance to a value that approaches that expected for the randomly oriented case.

(16) Swanson, B. I. Private communication.

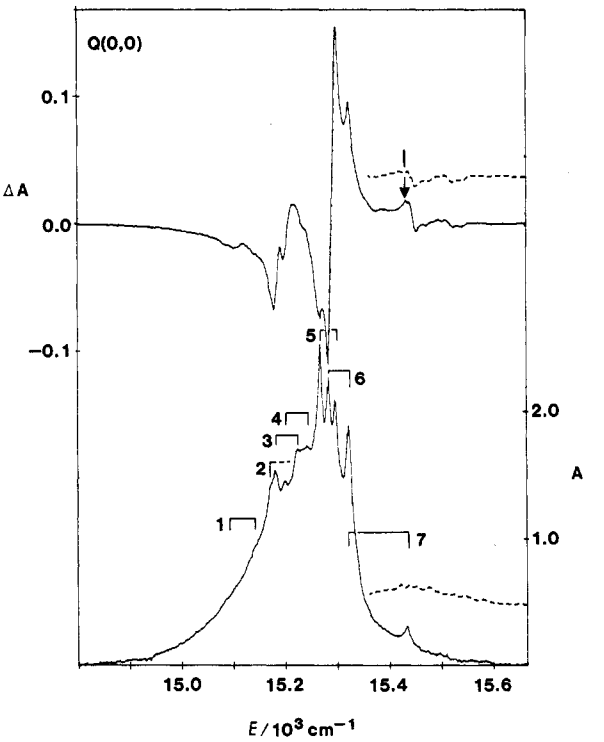

Figure 5. MCD (upper curve) and absorption spectra (lower curves) of ZnPc/Ar in the region of the Q(0,0) envelope, at ~5 K. A is the absorbance and ΔA is the MCD per tesla. The pairs of bands corresponding to each of the seven distinguishable sites of the matrix are indicated above the absorption spectrum. The weak, positive $\mathcal{B}$ term associated with site 7 is indicated by an arrow. The dashed curves are simulated vibronic spectra obtained by using the parameters in Table II and the empirical band shape of the Q(0,0) envelope. For further explanation see section V.1.

Experimentally, two types of dependence on θ are observed (section III), which gives strong evidence that the ZnPc molecules *are* preferentially orientated. If this is the case, then we must conclude that the spectra are dominated by $\pi \rightarrow \pi^*$ (${}^1A_{1g} \rightarrow {}^1E_u$) transitions. This is supported by the predominance of $\mathcal{A}$ (or pseudo-$\mathcal{A}$) terms in the MCD (Figures 5–10). In our subsequent discussion we assume complete preferential orientation.

3. Vibronic Transitions. Of the possible vibronic (vibrationally induced) transitions, the only ones that can be observed in the strongly oriented case are ${}^1A_{1g} \rightarrow {}^1E_u \otimes \gamma_g$, ${}^1\Gamma_g \otimes e_u$, ${}^1E_g \otimes \gamma_u$ and ${}^1\Gamma_u \otimes e_g$. (Here γ symbolizes an activating vibration of symmetry a_1, a_2, b_1, or b_2 and Γ an electronic state of one of these symmetries.) All of these can potentially show B terms, but only the transitions ${}^1A_{1g} \rightarrow {}^1E \otimes \gamma$ (with appropriate u and g subscripts) can give rise to $\mathcal{A}$ terms. If orientation is not complete, z-polarized vibronic transitions are possible but will only give rise to $\mathcal{B}$ terms.

For a vibronic $\mathcal{A}$ term corresponding to ${}^1A_{1g} \rightarrow {}^1E^a \otimes \gamma$, the experimentally measurable quantity is (eq 9 and 6)

$$\frac{\mathcal{A}_1^z({}^1E^a \otimes \gamma)}{\mathcal{D}_0^z({}^1E^a \otimes \gamma)} = 2i\langle({}^1E^a \otimes \gamma)x|L_z|({}^1E^a \otimes \gamma)y\rangle \quad (14a)$$

Here, the bra and ket functions, respectively, represent the x and y components of the vibronic state. Expansion of these functions according to eq 10.2.3 and 10.2.1 of ref 7 and the relationship $\langle Ex|L_z|Ey\rangle = -\langle Ey|L_z|Ex\rangle$ give

$$\frac{\mathcal{A}_1^z({}^1E^a \otimes \gamma)}{\mathcal{D}_0^z({}^1E^a \otimes \gamma)} = 2iS_\gamma\langle {}^1E^a x|L_z|{}^1E^a y\rangle \quad (14b)$$

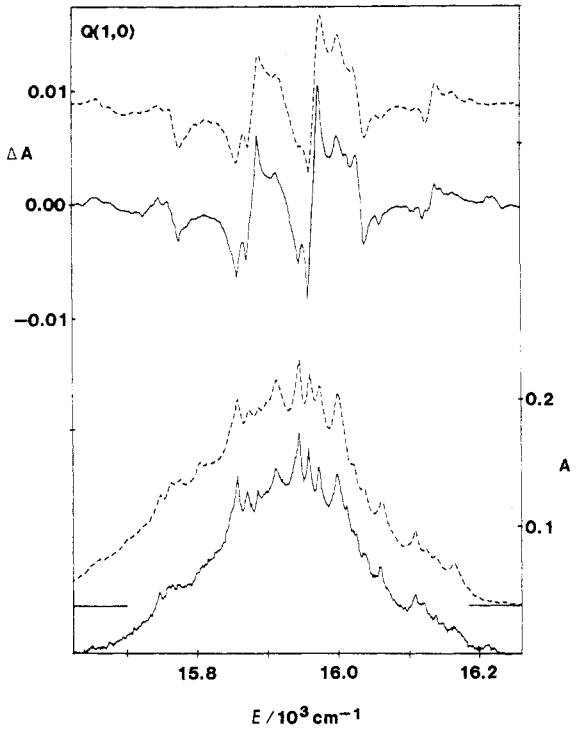

Figure 6. MCD (upper curve) and absorption spectra (lower curves) of ZnPc/Ar in the region of the Q(1,0) envelope, at ~5 K. The dashed curves are simulated vibronic spectra obtained by using the parameters in Table II and the empirical band shape of the Q(0,0) envelope. For further explanation see section V.1.

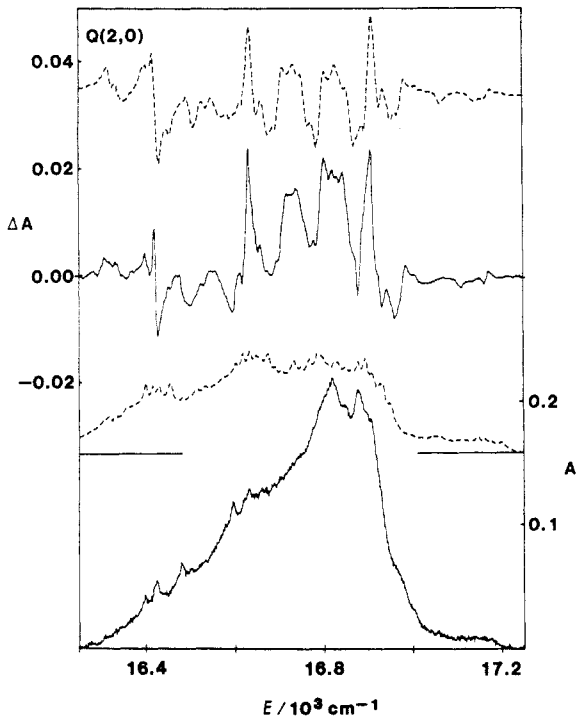

Figure 7. MCD (upper curve) and absorption spectra (lower curves) of ZnPc/Ar in the region of the Q(2,0) envelope, at ~5 K. The dashed curves are simulated vibronic spectra obtained by using the parameters in Table II and the empirical band shape of the Q(0,0) envelope. The large differences between the observed and simulated spectra give evidence for the presence of an underlying electronic transition. For further explanation see section V.1.

where the matrix element pertains to the unperturbed electronic states and the phase factor S_γ is given by

$$S_\gamma = \sum_{\lambda=x,y} (-1)^{\delta(\lambda,y)} (E^a\lambda \otimes \gamma|x)(y|E^a\bar{\lambda} \otimes \gamma) \qquad (15)$$

λ and $\bar{\lambda}$ are conjugate partner labels of the unperturbed electronic

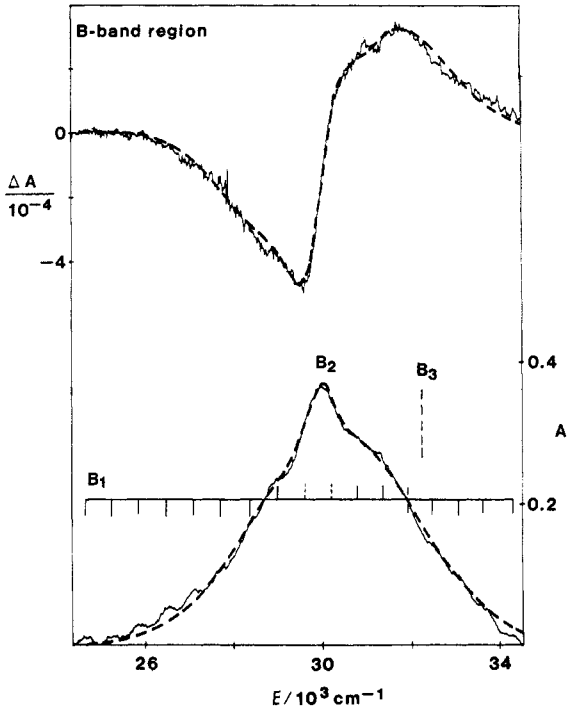

Figure 8. MCD (upper curve) and absorption spectrum of ZnPc/Ar in the B-band region, at ~5 K. The absorption spectrum comprises a strong broad band, designated B_1, and a weaker band, corresponding to the maximum of the region and designated B_2. B_1 exhibits a long progression with spacings of ~595 cm^{-1}. Overlapping $\mathcal{A}$ terms of these two transitions give rise to the overall positive $\mathcal{A}$ term observed in the MCD. The fit of the absorption and MCD by the sum of two Gaussians is shown by the dashed curves whose parameters are listed in Table V. A third band, B_3, is observed only when the matrix is rotated with respect to the optical axis (see section V.2 and Figure 4).

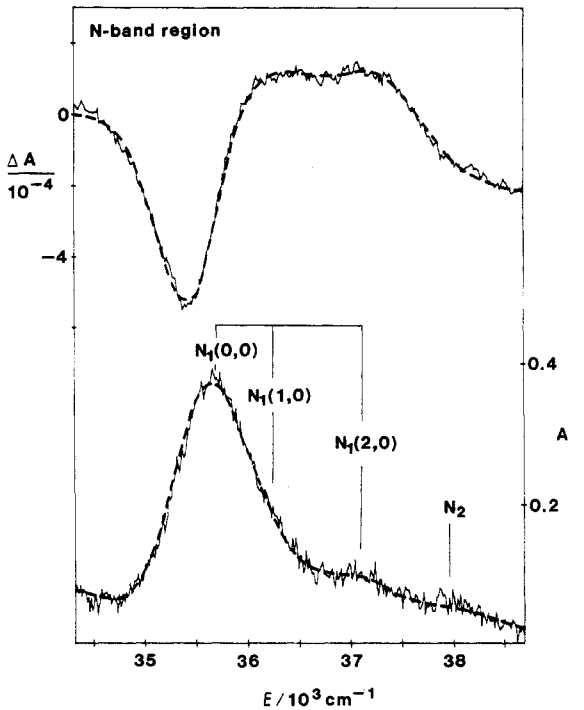

Figure 9. MCD (upper curve) and absorption spectrum of ZnPc/Ar in the N-band region, at ~5 K. $N_1(0,0)$ and N_2 are electronic origins. $N_1(1,0)$ and $N_1(2,0)$ are vibronic bands with shifts of 580 and 1410 cm^{-1}, respectively, from $N_1(0,0)$. The absorption due to $N_1(1,0)$ is largely obscured by overlap with $N_1(0,0)$, but its presence is verified by fitting both the absorption and MCD. The overall fits are shown by dashed curves, and the parameters are listed in Table V.

state, E^a, and the vector coupling coefficients relate the transformation properties of the vibronically coupled functions to those

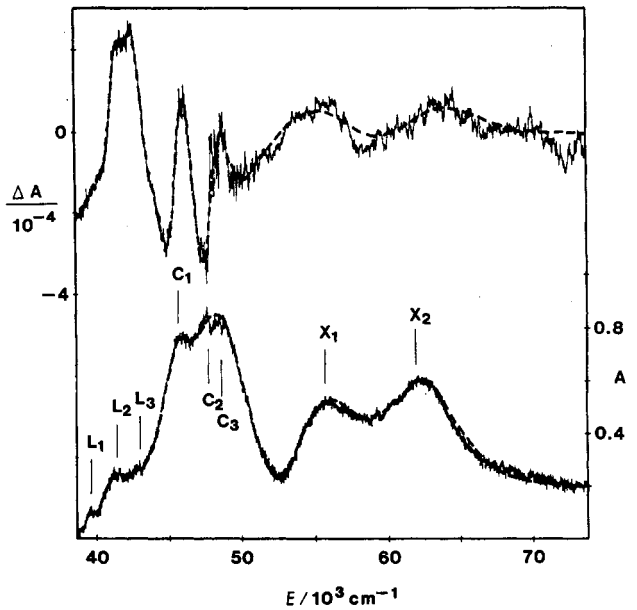

Figure 10. MCD (upper curve) and absorption spectrum of ZnPc/Ar in the vacuum ultraviolet. The band designations shown for the absorption spectra follow the discussion in section V. The overall fits are shown by the dashed curves, and the parameters are listed in Table V.

of the Cartesian x and y axes. The factor $(-1)^{\delta(\lambda,y)}$ is -1 when $\lambda = y$ and 1 when $\lambda = x$.

Evaluation of S_γ gives $S_{a_i} = 1$ and $S_{b_i} = -1$ with $i = 1$ or 2. Thus, for ${}^1A_{1g} \rightarrow {}^1E_u \otimes \gamma_g$, vibronic bands with $\gamma_g = a_{1g}$ or a_{2g} will show MCD $\mathcal{A}$ terms of the *same* sign (and the same $\mathcal{A}_1/\mathcal{D}_0$ ratio) as the electronic origin, while bands with $\gamma_g = b_{1g}$ or b_{2g} will show $\mathcal{A}$ terms of *opposite* sign. Similarly, ${}^1A_{1g} \rightarrow {}^1E_g$ is electronically forbidden, but ${}^1A_{1g} \rightarrow {}^1E_g \otimes \gamma_u$ will be vibronically allowed with $\gamma_u = a_{1u}$ or a_{2u} showing $\mathcal{A}$ terms of opposite sign to $\gamma_u = b_{1u}$ or b_{2u}.

4. Evaluation of Angular Momentum Matrix Elements. The theoretical determination of the MCD parameters of the preceding sections requires the evaluation of angular momentum matrix elements, the most important of which involve the operator L_z. These can ultimately be reduced to a sum of one-electron matrix elements of the form $\langle ex|l_z|ey'\rangle$, where $|ex\rangle$ and $|ey'\rangle$ represent molecular orbitals and l_z is the one-electron orbital angular momentum operator. In the case of $\mathcal{A}$ terms $|ex\rangle$ and $|ey'\rangle$ are degenerate ($y' = y$), whereas for $\mathcal{B}$ terms they are nondegenerate.

For π MOs that are linear combinations of $2p_z$ atomic orbitals, all single-center terms vanish, since $l_z^a|2p_z^a\rangle = 0$ at atomic center a. However, two-center terms do contribute and are entirely responsible for the observed angular momenta. The treatment of this case has been discussed previously.[17,18] The result in its most useful form[18] is (in units of $\hbar$)

$$\langle 2p_z^a|l_z^o|2p_z^b\rangle = -iT(a,b)(x_a y_b - y_a x_b) \tag{16}$$

where l_z^o is the one-electron orbital angular momentum operator at the molecular origin, and x_a and y_a are Cartesian coordinates of atom a with respect to the origin. $T(a,b)$ is an overlap integral of the form[18]

$$T(a,b) = 0.2\zeta^2 e^{-\zeta D}(1 + \zeta D + \tfrac{1}{3}(\zeta D)^2)[(1 - \tau^2)^{7/2}B] \tag{17a}$$

where

$$\zeta = (\zeta_a + \zeta_b)/2 \tag{17b}$$

$$\tau = (\zeta_a - \zeta_b)/(\zeta_a + \zeta_b) \tag{17c}$$

$$B = 15[(\tau\zeta D)^2 \sinh(\tau\zeta D) - 3\tau\zeta D \cosh(\tau\zeta D) + 3 \sinh(\tau\zeta D)]/(\tau\zeta D)^5 \tag{17d}$$

(17) Stephens, P. J.; Suëtaka, W.; Schatz, P. N. *J. Chem. Phys.* **1966**, *44*, 4592–4602.

(18) McHugh, A. J.; Gouterman, M.; Weiss, C. *Theoret. Chim. Acta* **1972**, *24*, 346–370.

TABLE I: Inequivalent Sites and Band Energies[a] of the Q(0,0) Envelope of ZnPc/Ar at ~5 K

site	$\mathcal{E}^-$/cm^{-1}	$\mathcal{E}^+$/cm^{-1}	Δ/cm^{-1}
1	15088	15140	52
2	15172	[c]	
3	15182	15225	43
4	15199	15241	42
5	15267	15296	29
6	15282	15322	40
7	15322[b]	15433	111

[a] $\mathcal{E}^-$ and $\mathcal{E}^+$ respectively represent the energies of the bands corresponding to negative and positive $\mathcal{B}$ terms. $\Delta = \mathcal{E}^+ - \mathcal{E}^-$. [b] Underlies the stronger $\mathcal{E}^-$ band of site 6. [c] Obscured by overlap with sites 4 and 5.

ζ_a is a screening constant for a Slater-type orbital ($R_a(2p_z^a) \propto r_a e^{-\zeta_a r_a}$), and D is the distance (in atomic units) between atoms a and b. In the case that $\zeta_a = \zeta_b$ (two carbon atoms, for example) $T(a,b)$ has a much simpler form where the factor in square brackets in eq 17a reduces to unity. (Note that in an equation quoted elsewhere[19] the angle $\angle oab$ must be defined as the counterclockwise rotation that takes the line segment $\overline{ab}$ onto $\overline{ao}$. This is required to ensure that $\langle 2p_z^a|l_z^o|2p_z^b\rangle = -\langle 2p_z^b|l_z^o|2p_z^a\rangle$.)

5. MCD Parameters from Molecular Orbital Models. With use of 16 and 17, given appropriate LCAO coefficients, it is a straightforward matter to calculate the MCD parameter ratios for an excitation between MOs. For example, consider the fully allowed $\pi \rightarrow \pi^*$ transition, ${}^1A_{1g} \rightarrow {}^1E_u^a$. This can only arise from the MO excitations $e_g \rightarrow \gamma_u$ or $\gamma_u \rightarrow e_g$. It then follows from eq 9a and the reduced form[7] of eq 6a that

$$\frac{\mathcal{A}_1^z({}^1E_u^a)}{\mathcal{D}_0^z({}^1E_u^a)} = \frac{2\bar{\mathcal{A}}_1({}^1E_u^a)}{\bar{\mathcal{D}}_0({}^1E_u^a)} = 2iS_{\gamma_u}\langle e_g x|l_z|e_g y\rangle \tag{18}$$

S_{γ_u} is in fact the same phase factor given in eq 15 and takes the value 1 for $\gamma_u = a_{iu}$ or -1 for $\gamma_u = b_{iu}$ ($i = 1$ or 2). Thus, if the MCD of an electronic transition is dominated by a single excitation, the sign alone of the $\mathcal{A}$ term gives important information.

In practice it is necessary to take configuration interaction (CI) into account. We can write a mixed-configuration state as

$$|{}^1E_u^A\rangle = \sum_k C_{kA}|{}^1E_u^k\rangle$$

where the C_{kA} are CI coefficients and the kets on the right-hand side denote single-configuration states. Then

$$\langle {}^1E_u^A x|L_z|{}^1E_u^A y\rangle = \sum_k |C_{kA}|^2\langle {}^1E_u^k x|L_z|{}^1E_u^k y\rangle + 2i \operatorname{Im} \sum_{j>k} C^*_{kA}C_{jA}\langle {}^1E_u^k x|L_z|{}^1E_u^j y\rangle \tag{19}$$

Since L_z is a sum of one-electron operators, the cross terms in eq 19 can be nonzero *only* when the excitations giving rise to $|{}^1E_u^k\rangle$ and $|{}^1E_u^j\rangle$ either originate or terminate at the same MO. In such cases, the relative contribution of the cross terms can be large. For example, for $|{}^1E_u^k(2a_{1u} \rightarrow 6e_g)\rangle$ and $|{}^1E_u^j(4a_{2u} \rightarrow 6e_g)\rangle$ the off-diagonal matrix element reduces to $-\langle 2a_{1u}|l_z|4a_{2u}\rangle$, which is of similar magnitude to the diagonal elements $\langle {}^1E_u^k x|L_z|{}^1E_u^k y\rangle = -\langle {}^1E_u^j x|L_z|{}^1E_u^j y\rangle = \langle 6e_g x|l_z|6e_g y\rangle$ (see later). Hence the angular momenta obtained from eq 19 can be much larger or much smaller (depending on the phase of $C^*_{kA}C_{jA}$) than one would expect from the diagonal terms alone.

V. Discussion of Spectra

1. Q-Band Region (14 700–17 200 cm^{-1}). The Q-band region is the one most extensively studied in the spectra of all Pc's, including ZnPc.[1-3,5,6,14,15] It includes three major band envelopes, traditionally labeled Q(0,0), Q(1,0), and Q(2,0). The most intense of these corresponds to the fully allowed ${}^1A_{1g} \rightarrow {}^1E_u^Q$ transition, which arises predominantly from the π(HOMO) $\rightarrow \pi^*$(LUMO) excitation[9] (Figure 11).

(19) Snyder, P. A.; Lund, P. A.; Schatz, P. N.; Rowe, E. M. *Chem. Phys. Lett.* **1981**, *82*, 546–551.

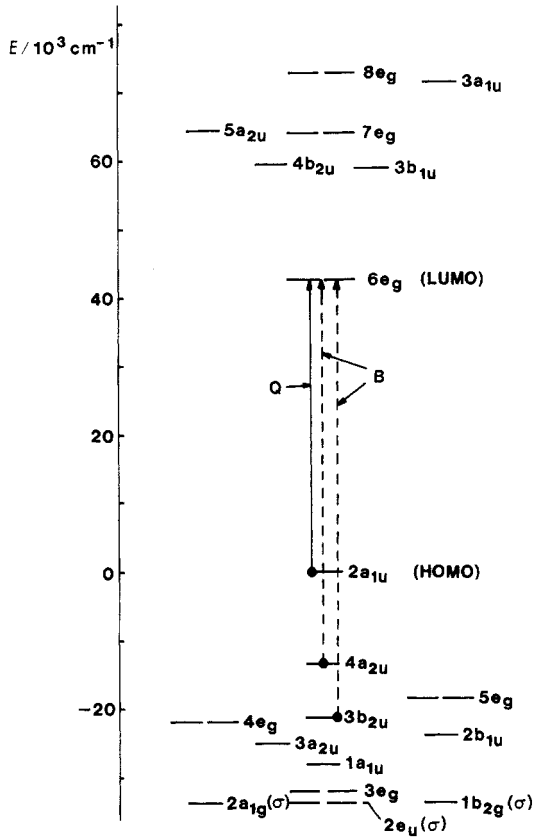

Figure 11. Higher lying occupied and lower lying unoccupied molecular orbitals of phthalocyanine according to ref 9. Numbering of the e_g, a_{1g}, and b_{2g} orbitals is reduced by one compared with ref 9 because of the omission of d-orbitals. The σ-orbitals, $2e_u$, $2a_{1g}$, and $1b_{2g}$, are $n(N_{p_\sigma})$ involving the lone pairs of the bridging nitrogen atoms. The zero energy is arbitrarily chosen to coincide with the HOMO. The Q(0,0) band excitation (full arrow) and major contributors to the B_1 and B_2 bands (dashed arrows) are indicated.

Figure 5 shows the absorption (lower) and MCD (upper) spectra of the Q(0,0) envelope. At least 12 peaks and shoulders are discernible in absorption (Table I), each of which corresponds to a maximum or a minimum in the MCD. Although the overall appearance of the MCD is that of a positive $\mathcal{A}$ term, it is clear that the individual transitions correspond to $\mathcal{B}$ terms. This observation is completely consistent with the existence of a crystal-field-stabilized Jahn–Teller effect proposed to explain doublet structure observed in the excitation spectra of metallophthalocyanines (MPc) in Shpol'skii matrices.[5] The splitting of a doubly degenerate excited state gives rise to a pair of $\mathcal{B}$ terms of opposite sign but equal magnitude. Overlap of these $\mathcal{B}$ terms results in a derivative-shaped pseudo-$\mathcal{A}$ term[7]. When the absorption bands that give rise to negative $\mathcal{B}$ terms are paired with bands giving rise to positive $\mathcal{B}$ terms (Figure 5), it becomes clear that the observed spectrum arises from the superposition of the transitions of seven major inequivalent sites. As for MPc's in Shpol'skii matrices,[5] the splitting seems to be very sensitive to the external environment of the complex, varying from 29 cm^{-1} for site 5 to 111 cm^{-1} for site 7 (Table I).

The MCD features between ~15 300 and 15 700 cm^{-1}, on the blue edge of the Q(0,0) envelope (Figure 5), are not readily accounted for by the above explanation. In particular, the absorption band at 15 433 cm^{-1} is assigned to the high-energy component of site 7 (Table I), which is expected to show a positive $\mathcal{B}$ term. In contrast, the dominant MCD feature in this region is a negative pseudo-$\mathcal{A}$ term. Following section IV.3, a_{ig} vibrational modes (i = 1 or 2) built on Q(0,0) will give rise to positive $\mathcal{A}$ (or pseudo-$\mathcal{A}$) terms, while b_{ig} activating modes will give rise to negative $\mathcal{A}$ (or pseudo-$\mathcal{A}$) terms. In fact, the MCD to the blue of 15 350 cm^{-1} in Figure 5 can be almost completely accounted for by the presence of b_{ig} overtones of 154 and 225 cm^{-1} and an a_{ig} overtone of 258 cm^{-1} (Table II). The dashed curves

TABLE II: Vibronically Active Vibrational Modes of the Q-Band Region

mode	$\mathcal{D}_0/\mathcal{D}_0(Q(0,0))^a$	$h\nu/cm^{-1b}$	S_γ	γ
ν_1	0.050	154	−1	b_{ig}
ν_2	0.020	255	−1	b_{ig}
ν_3	0.015	258	1	a_{ig}
ν_4	0.015	479 (478)	−1	b_{ig}
ν_5	0.023	589 (587)	1	a_{ig}
ν_6	0.057	676 (676)	1	a_{ig}
ν_7	0.023	739 (742)	−1	b_{ig}
ν_8	0.015	840 (840)	1	a_{ig}
ν_9	0.016	1133 (1143)	−1	b_{ig}
ν_{10}	0.004	1215 (1206)	−1	b_{ig}
ν_{11}	0.010	1334 (1332)	1	a_{ig}
ν_{12}	0.010	1350	−1	b_{ig}
ν_{13}	0.008	1408 (1412)	1	a_{ig}
ν_{14}	0.005	1466 (1477)	−1	b_{ig}
ν_{15}	0.008	1500 (1492)	1	a_{ig}
ν_{16}	0.006	1565	−1	b_{ig}
ν_{17}	0.015	1600	1	a_{ig}
ν_{18}	0.010	1628	−1	b_{ig}
ν_{19}	0.005	1684	1	a_{ig}
ν_{20}	0.002	1879	1	a_{ig}

[a] $\mathcal{D}_0(Q(0,0))$ is the dipole strength of the entire Q(0,0) envelope. [b] Values in parentheses are from ref 5.

in Figure 5 are simulated vibronic spectra obtained by using the empirical band shape of the Q(0,0) envelope and the parameters of Table II. The simulated and observed absorption spectra do not agree closely because of strong overlap with the Q(0,0) component at 15 433 cm^{-1}. The relatively weak contribution to the MCD from this latter band arises from the fact that the MCD of the Q(0,0) envelope comprises pseudo-$\mathcal{A}$ terms. The intensity of a pseudo-$\mathcal{A}$ term is inversely proportional to the splitting of the two components of the Q(0,0) transition, and site 7 (Table I) exhibits a splitting more than twice as large as any other site. The weak positive $\mathcal{B}$ term corresponding to site 7 lies just to the red of the stronger negative pseudo-$\mathcal{A}$ term and is indicated by an arrow in Figure 5.

The Q(1,0) MCD and absorption envelopes are also amenable to a vibronic interpretation. In Figure 6 the observed spectra are compared with simulated spectra (dashed curves) obtained by using the Q(0,0) band shape and the parameters of Table II. It clearly shows that the whole of the Q(1,0) region can be accounted for in terms of vibronic bands.

In the Q(2,0) region (Figure 7) a vibronic analysis does not give a complete account of the observed data. Although the spectra simulated according to the parameters of Table II (dashed spectra, Figure 7) do reproduce much of the finer structure, they fail to account for most of the absorption intensity as well as the positive MCD intensity observed near the center of this region. Subtraction of the simulated curves from the observed spectra suggests the additional presence of a separate electronic band (referred to as Q′ in the following), which shows a positive $\mathcal{B}$ term in the MCD. A similar conclusion was reached by Huang et al. using selective excitation spectroscopy in Shpol'skii matrices.[6] These workers assigned Q′ to an allowed $e_u(N_{p_\sigma}) \rightarrow 6e_g$ transition, which also involves vibronic borrowing from Q(0,0) via e_g modes. Such an assignment is consistent with a $\mathcal{B}$-term dominated MCD, as we discuss further in section VI.

Despite the presence of the Q′ band, the agreement between the structure of the observed and simulated MCD spectra of Figures 5–7 gives us confidence in the parameters of Table II. Most of the vibrational frequencies obtained from the simulation are in very close accord with those of the strongest vibronic bands observed by Huang et al. in the excitation spectrum of ZnPc in a Shpol'skii matrix.[5] The MCD sign (i.e., the sign of S_γ in eq 14b) allows us to determine the symmetries (a_{ig} or b_{ig}) of the active vibrational mode.

Equations 3a and 3b are invariant to first-order effects (unitary transformations of the basis set) such as crystal-field splittings or Jahn–Teller couplings, provided the numerical integrations cover the entire band envelope described by the basis set. In this case

the basis spans the entire vibronic manifold accompanying the electronic transition $^1A_{1g} \rightarrow {}^1E_u^Q$, and the natural range of integration is over the entire Q(0,0), Q(1,0), Q(2,0) region. However, as mentioned above, Q(2,0) arises in part from an additional *electronic* transition. This invalidates the theoretical significance of such an integration.

A similar invariance applies if only the 0 → 0 (no-phonon) contribution to $^1A_{1g} \rightarrow {}^1E_u^Q$ is considered. Since Q(0,0) is overwhelmingly dominated by such transitions *and* since Q(1,0) and Q(2,0) have only a few percent of the integrated intensity of Q(0,0), a negligible error results if the analysis is carried out over Q(0,0) only. The results so obtained are $\mathcal{A}_1(Q)/\mathcal{D}_0(Q) = 4.2$ and $\mathcal{B}_0(Q)/\mathcal{D}_0(Q) = -4.9 \times 10^{-3}$ cm. The strong predominance of the $\mathcal{A}$-term parameter is to be expected for $^1A_{1g} \rightarrow {}^1E_u^Q$. Integration over the Q(2,0) region gives $\mathcal{B}_0/\mathcal{D}_0 = 1.6 \times 10^{-2}$ cm, which is about 3 times the absolute value obtained for Q(0,0) and arises almost entirely from the transition $^1A_{1g} \rightarrow Q'$.

2. B-Band Region (24 000–34 500 cm^{-1}). The B-band (or Soret band) of MPc has been previously assigned as being fully allowed, $^1A_{1g} \rightarrow {}^1E_u^B$. In fact HRS calculate two strongly allowed $\pi \rightarrow \pi^*$ transitions near the B-band region,[9] both of which contain strong admixtures of excitations terminating in the $6e_g$ MO. They also predict,[9,20] along with Gouterman and his co-workers,[18,21] that an allowed $n(N_{p_\sigma}) \rightarrow \pi^*$ transition should lie in the B-band region.

Our experimental results are entirely consistent with the calculations cited above. At the red end of the region (Figure 8) we observe an origin (24 680 cm^{-1}) followed by a progression of bands with spacings of 595 ± 6 cm^{-1}. Seven members of this progression are evident before the maximum (at 30 200 cm^{-1}), with a probable seven further members observed after the maximum. The band maximum, at 29 950 cm^{-1}, does not fit into this pattern, and we believe it corresponds to a separate electronic transition. Overlapping $\mathcal{A}$ terms from these two transitions (referred to as B_1 and B_2 hereafter) give rise to a broad, positive $\mathcal{A}$ term, with $\mathcal{A}_1/\mathcal{D}_0 = 4.4$ obtained by integration over the full range of Figure 8. The absorption spectrum obtained with $\theta = \pi/6$ (dotted line, Figure 4) reveals a third band, B_3, at 32 200 cm^{-1}. According to the discussion of section IV.2, this corresponds to a *z*-polarized transition and is almost certainly $n(N_{p_\sigma}) \rightarrow \pi^*$. (It should be emphasized that multiple sites will not be observable in the B-band or higher energy regions due to the much greater inherent vibronic line widths. For example, inspection of Figure 5 shows that if line widths in the Q(0,0) band were of the order of only 50–100 cm^{-1}, rather than ~10 cm^{-1}, the band would have a smooth envelope since the half-width of the entire band is ~200 cm^{-1}. In the higher energy regions the presence of multiple sites simply broadens somewhat any vibronic structure that is resolved.)

Rough estimates of the spectral parameters of these bands can be obtained by fitting the data with eq 1 and 2, by using a Gaussian band-shape function. Good fits (dashed curves) to the absorption spectrum of Figure 8 are obtained by using two Gaussian curves, an intense, broad band corresponding to B_1 and a weaker, sharper band corresponding to B_2. Similarly, good fits to the MCD are obtained with $\mathcal{A}$ and $\mathcal{B}$ terms centered at the same energies, and these yield the parameter ratios $\mathcal{A}_1(B_1)/\mathcal{D}_0(B_1) = 4.3$, $\mathcal{B}_0(B_1)/\mathcal{D}_0(B_1) = -1.2 \times 10^{-4}$ cm, $\mathcal{A}_1(B_2)/\mathcal{D}_0(B_2) = 3.7$, and $\mathcal{B}_0(B_2)/\mathcal{D}_0(B_2) = -2.4 \times 10^{-3}$ cm.

Whereas Nyokong et al. attempted to restrict the subjectivity of their fitting procedure by holding the band width and barycenter parameters constant between absorption and MCD,[1] we find it necessary to assign a significantly narrower band width (by a factor of 0.79) to the MCD corresponding to B_1. We have interpreted this requirement as indicating the presence of pseudo-$\mathcal{A}$ terms, rather than true $\mathcal{A}$ terms, in the MCD. This interpretation is supported by simulation and fitting of a pseudo-$\mathcal{A}$ term and its corresponding absorption. For example, a simulated absorption band composed of two Gaussian curves that are identical, apart from a relative displacement equal to their half-width at $1/e$ maximum (HW1/*e*M), can be reasonably well fit with a single Gaussian. Likewise, the corresponding simulated MCD pseudo-$\mathcal{A}$ term can be satisfactorily fit with a single Gaussian $\mathcal{A}$ term. However, the line width obtained from the MCD fit is 0.85 of the value obtained from the absorption. The presence of pseudo-$\mathcal{A}$ terms is not unexpected in light of the results for the Q-band region (section V.1).

The spacing of the progression observed in the B_1 band (595 ± 6 cm^{-1}) is similar to the energy of the vibronically important ν_5 (a_{ig}) vibration of the Q-band region (Table II). However, there is strong evidence that this is not the only progression building mode of the B_1 band. Using a semiclassical model and assuming a single progression-building mode, the displacement of the excited state with respect to the ground state can be quantified by the Huang–Rhys parameter, *S*, of eq 20.

$$S = (\bar{\mathcal{E}} - \mathcal{E}_0)/h\nu \tag{20}$$

$\mathcal{E}_0$ is the energy of the band origin and $h\nu$ is the vibrational energy. With $\bar{\mathcal{E}}(B_1) = 30\,200$ cm^{-1} obtained by fitting, eq 20 gives $S = 9.3$ for a mode with $h\nu = 595$ cm^{-1}. This value, however, is at odds with a further expectation from the semiclassical theory:[22]

$$I_1 = SI_0 \tag{21}$$

where I_0 and I_1 are respectively the intensities of the origin and the first member of the progression. Equation 21 and Figure 8 indicate that *S* can be no greater that ~1.5, and it is clear that there must be at least one further progression-building mode. The available data are not sufficient for us to make a detailed analysis of the B_1 band shape, but we note that E_u states in the D_{4h} point group are susceptible to a Jahn–Teller effect in b_{1g} and b_{2g} vibrational modes. Progression-building modes can therefore be of a_{1g}, b_{1g}, or b_{2g} symmetry.

Moment analysis of the data in Figure 4 yields the results $\bar{E}(B_3) = 32\,200$ cm^{-1} and $A_{\pi/6}^z(B_3) = 0.15A_0^z(B_1)$. After applying eq 13b and averaging over all possible orientations, the second of these results leads to the conclusion that the B_3 band should account for about 30% of the absorbance observed in the B-band region of the spectra of gas-phase or solution samples. Additionally, our assignment of B_3 to a transition of the type $^1A_{1g} \rightarrow {}^1A_{2u}$ indicates that the corresponding contribution to the MCD should consist purely of a $\mathcal{B}$ term. These predictions are in excellent accord with the results of Nyokong et al.[1] Their solution spectra of ZnPc with cyanide and imidazole ligands were, respectively, fitted with four and five bands in the B-band region. (The greater number of bands that they observe may be a result of the presence of the additional ligands.) For both complexes they observe bands in the vicinity of B_3 (33 322 cm^{-1} for cyanide, and 31 933 and 34 008 cm^{-1} for imidazole), which show pure $\mathcal{B}$ terms and respectively contribute 29% and 27% to the total absorbance of the B-band region.

3. N-Band Region (34 500–38 500 cm^{-1}). The N-band spectra (Figure 9) were obtained by using synchrotron radiation. HRS[9] calculate very little dipole strength in this region, and indeed we observe bands that are relatively weak in comparison with the B-band region (Figure 2).

The absorption spectrum clearly shows a relatively strong band at 35 610 cm^{-1}, followed by weaker bands at 37 020 and 37 920 cm^{-1}. Fits (dashed curves) to both the absorption and the MCD (maintaining the same band-width parameters in both cases) reveal a fourth band centered at 36 190 cm^{-1}. The MCD has the overall appearance of a positive $\mathcal{A}$ term, and the ratio $\mathcal{A}_1(N)/\mathcal{D}_0(N) = 1.4$ is obtained by moment analysis over the range of Figure 9.

The results of fitting show the three lower energy bands to have very similar band widths (HW1/*e*M ~ 490 cm^{-1}) and positive $\mathcal{A}$ terms with $\mathcal{A}_1/\mathcal{D}_0$ ratios of 1.1, 1.3, and 0.7 from lower to higher energy. The second and third bands are shifted by 580 and 1410 cm^{-1} from the first. These shifts are very close to the

(20) Henriksson, A.; Sundbom, M. *Theoret. Chim. Acta* **1972**, *27*, 213–222.
(21) Schaffer, A. M.; Gouterman, M. *Theoret. Chim. Acta* **1972**, *25*, 62–82.
(22) Wilson, R. B.; Solomon, E. I. *J. Am. Chem. Soc.* **1980**, *102*, 4085–4095.

energies of the vibronically active $\nu_5(a_{ig})$ and $\nu_{13}(a_{ig})$ modes of the Q-band region (Table II). We believe that these three bands constitute the origin and two vibronic overtones of the same electronic transition and have denoted them $N_1(0,0)$, $N_1(1,0)$, and $N_1(2,0)$ in analogy with the established nomenclature for the Q-band region.

The band at 37 920 cm^{-1} (N_2) is ~50% broader than the others and corresponds to a negative $\mathcal{A}$ term in the MCD. We have assigned it to a separate electronic transition, $^1A_{1g} \rightarrow {}^1E_u^{N_2}$. The ratios $\mathcal{A}_1(N_2)/\mathcal{D}_0(N_2) = -1.4$ and $\mathcal{B}_0(N_2)/\mathcal{D}_0(N_2) = -2.0 \times 10^{-3}$ cm were obtained by fitting.

4. L-Band Region (38 500–44 000 cm^{-1}). HRS[9] calculate fairly weak transitions in the vicinity of the L-band region (Figure 2). In the absorption spectrum, obtained with synchrotron radiation (Figures 2 and 10), the L-band region appears as a broad, rather weak and featureless shoulder on the red side of the stronger C-band region.

Absorption bands are clearly evident at 39 400 and 41 100 cm^{-1}, and there is a hint of a third band at 43 000 cm^{-1} (Figure 10). The presence of the third band is supported by the MCD, where the zero-crossing at the same energy infers the presence of a negative $\mathcal{A}$ (or pseudo-$\mathcal{A}$) term. We consider these three bands to arise from separate electronic transitions and denote them L_1, L_2, and L_3 in the following discussion.

Strong overlap between the L bands and with bands in neighboring regions limits the quantitative usefulness of fitting in this case. However, fits should provide qualitatively reliable information concerning the signs of the MCD parameters. In fact, we are able to obtain fits (dashed curves) that look quite reasonable. The resulting parameter ratios are $\mathcal{A}_1(L_1)/\mathcal{D}_0(L_1) = 7.0$, $\mathcal{A}_1(L_2)/\mathcal{D}_0(L_2) = 0.4$, and $\mathcal{A}_1(L_3)/\mathcal{D}_0(L_3) = -1.3$. The first of these ratios seems rather too large, and we do not regard it as being reliable. As was the case for the B_1 band, it is necessary to fit the MCD of the L_2 and L_3 bands with smaller band widths than the absorption, and we suspect the presence of pseudo-$\mathcal{A}$ terms.

5. C-Band Region (44 000–52 500 cm^{-1}). We have previously reported spectra in this region[10] but now believe our earlier data to be largely erroneous (section VIII).

HRS[9] calculate a number of relatively strong transitions to lie in this region of the spectrum, and indeed the C bands appear to be the strongest outside the B-band region (Figure 2). Broad bands at 45 320 (C_1) and 48 370 cm^{-1} (C_3) are evident in the absorption spectrum (Figure 10). C_1 is clearly associated with a positive $\mathcal{A}$ term in the MCD. Another positive $\mathcal{A}$ term, at 47 720 cm^{-1}, is too narrow to be assigned to C_3 and indicates the presence of a third transition, C_2. C_3 appears to be associated with a negative $\mathcal{A}$ term, part of the negative lobe of which can be seen near 50 000 cm^{-1} (Figure 10).

Fitting (dashed curves) of the C-band region with eq 1 and 2 and a Gaussian band-shape function yield the parameters $\mathcal{A}_1(C_1)/\mathcal{D}_0(C_1) = 0.6$, $\mathcal{B}_0(C_1)/\mathcal{D}_0(C_1) = -2.8 \times 10^{-4}$ cm, $\mathcal{A}_1(C_2)/\mathcal{D}_0(C_2) = 8.8$, $\mathcal{B}_0(C_2)/\mathcal{D}_0(C_2) = -4.7 \times 10^{-3}$ cm, $\mathcal{A}_1(C_3)/\mathcal{D}_0(C_3) = -0.4$, and $\mathcal{B}_0(C_3)/\mathcal{D}_0(C_3) = -3.7 \times 10^{-4}$ cm. We again emphasize that the magnitudes of these ratios may not be reliable because of strong overlap between bands, but we believe the signs to be correct. In particular, it is clear that $\mathcal{A}_1(C_2)/\mathcal{D}_0(C_2)$ must be positive since C_2 definitely shows a positive $\mathcal{A}$ term in the MCD. However, overlap between C_2 and the broader, more intense C_1 and C_3 bands makes a precise determination of $\mathcal{D}_0(C_2)$ very difficult, and it seems likely that the ratio $\mathcal{A}_1(C_2)/\mathcal{D}_0(C_2) = 8.8$ is too large.

6. X-Band Region (52 500–70 000 cm^{-1}). The X-band region lies above the highest energy transition calculated by HRS[9] (Figure 2). It contains two broad and relatively intense bands, centered at 55 600 and 61 900 cm^{-1} and denoted X_1 and X_2, respectively (Figure 10). The progression of sharp bands that were seen to dominate this region of ZnPc/Ar spectra in an earlier report[10] we now believe to arise from the presence of an impurity (section VIII).

The MCD associated with bands X_1 and X_2 is broad and rather weak. The parameter ratios $\mathcal{A}_1(X_1)/\mathcal{D}_0(X_1) = 0.0$, $\mathcal{B}_0(X_1)/\mathcal{D}_0(X_1) = 2.5 \times 10^{-4}$ cm, $\mathcal{A}_1(X_2)/\mathcal{D}_0(X_2) = 0.8$, and $\mathcal{B}_0(X_2)/\mathcal{D}_0(X_2) = 8.9 \times 10^{-5}$ cm were obtained by fitting (dashed curves).

TABLE III: Values of the Matrix Elements $i\langle a|l_z|b\rangle$ from Ref 2 with Use of Slater Orbitals and the ω Technique

	b							
a	$4e_gy$	$5e_gy$	$6e_gy$	$7e_gy$	$8e_gy$	$3a_{2u}$	$4a_{2u}$	$4b_{2u}$
$4e_gx$	−0.85							
$5e_gx$		0.24						
$6e_gx$			1.35					
$7e_gx$				−0.42				
$8e_gx$					0.46			
$1a_{1u}$						0.05	0.68	
$2a_{1u}$						−1.76	1.18	
$3b_{1u}$								−1.15

VI. Comparison with the MO Treatment of HRS[9]

The treatment of Henriksson et al.[9] (HRS) is based on a semiempirical SCF MO method (Peel method) and is described in ref 9 and references therein. The explicit case treated by HRS is CuPc; we have removed the Cu d-orbitals in our discussion and comparisons. In Figure 11 we show (drawn to scale) the energies of the relevant MOs calculated by HRS. The numbering of e_g, a_{1g}, and b_{2g} orbitals in Figure 11 is reduced by one in comparison with HRS due to the removal of d-orbitals.

To evaluate the MO angular momentum matrix elements of eq 18, the LCAO (linear combination of atomic orbitals) coefficients of each MO are required. Unfortunately, HRS list only the atomic populations (the sums of squares of the LCAO coefficients over the x and y components of each state), and thus the $\langle ex|l_z|ey\rangle$ matrix elements cannot be evaluated from their published results by using eq 16. We have estimated the magnitudes of these and related matrix elements using a simpler iterative method, the ω technique.[23] The details of the calculation are discussed elsewhere,[2] and we simply list the matrix elements relevant to our discussion in Table III.

An important point arising from section IV.5 is that configuration interaction (CI) must be considered in any quantitative attempt to evaluate $\mathcal{A}_1/\mathcal{D}_0$. HRS[9] give the largest CI coefficients of several excited states, which should, in principle, allow us to estimate the terms of eq 19. However, the fact that they do not list the individual LCAO coefficients prevents us from relating the phases of the matrix elements in Table III to those that would be obtained from the wave functions of the HRS calculation. Thus, we can estimate the absolute magnitudes but cannot determine the signs of the individual terms that contribute to the second sum in eq 19.

Tentative correlations between the observed and calculated spectra are listed in Table IV and are discussed below, starting from the red end of our spectra and progressing to higher energy. HRS did not extend calculations as far as the X-band region, and that region is not discussed in this section. The "observed" parameters of Table IV are those determined from the experimental data as described in section V. The "calculated" $\mathcal{A}_1^z/\mathcal{D}_0^z$ parameters are derived by using the CI coefficients of HRS and the matrix elements of Table III, in light of our discussion above. The column headed "diag" gives the contribution to $\mathcal{A}_1^z/\mathcal{D}_0^z$ that arises from the first (diagonal) term of eq 19. The column headed "inter" gives the sum of the absolute values of the individual terms that contribute to the second (interference) term of eq 19 and can be regarded as an estimate of the maximum degree to which the calculated value can deviate from the "diagonal" value.

HRS predict that the Q(0,0) band is dominated by the excitations $2a_{1u} \rightarrow 6e_g$ and $4a_{2u} \rightarrow 6e_g$, with respective contributions of ~79% and ~16%. In the absence of CI we note (eq 18) that $\mathcal{A}_1^z/\mathcal{D}_0^z$ has precisely the same value, $2i\langle 6e_gx|l_z|6e_gy\rangle \sim 2.7$ (Table III), for each of these excitations. After allowing for CI, these excitations make a combined diagonal contribution of $0.95 \times 2.7 \sim 2.6$ and an additional interference contribution of absolute

(23) Streitwieser, A., Jr. *Molecular Orbital Theory for Organic Chemists*; Wiley: New York, 1961; Chapters 1–4.

TABLE IV: Correlations between Observed Spectra of ZnPc/Ar and the Calculated Spectrum of HRS[9]

band	$\mathcal{E}/10^3$ cm^{-1} obsd	$\mathcal{E}/10^3$ cm^{-1} calcd	$\mathcal{A}_1^z/\mathcal{D}_0^z$ obsd[a]	$\mathcal{A}_1^z/\mathcal{D}_0^z$ calcd diag[b]	$\mathcal{A}_1^z/\mathcal{D}_0^z$ calcd inter[c]	$\mathcal{D}_0^z/\mathcal{D}_0^z(Q)$[a,d] obsd[a]	$\mathcal{D}_0^z/\mathcal{D}_0^z(Q)$[a,d] calcd[e]	assignment
Q	15.23	18.4	4.2	2.6	1.7	1.00	1.00	$^1A_{1g} \rightarrow {}^1E_u$
Q′	16.78	31.4	0	0	0	0.07	0.00	$^1A_{1g} \rightarrow {}^1A_{2u}$
B_1	30.20	34.5	4.3	0.4	1.3	1.58	2.55	$^1A_{1g} \rightarrow {}^1E_u$
B_2	29.95	35.3	3.7	0.5	1.3	0.05	1.66	$^1A_{1g} \rightarrow {}^1E_u$
B_3	32.20	42.3	0	0	0	0.00	0.00	$^1A_{1g} \rightarrow {}^1A_{2u}$
N_1	35.61	36.6	1.1	0.7	0.0	0.12	0.01	$^1A_{1g} \rightarrow {}^1E_u$
N_2	37.92	40.1	−1.4	*f*	*f*	0.02	0.00	$^1A_{1g} \rightarrow {}^1E_u$
L_1	39.40	42.9	7.0	*f*	*f*	0.01	0.00	$^1A_{1g} \rightarrow {}^1E_u$
L_2	41.10	47.7	0.4	0.5	0.0	0.09	0.10	$^1A_{1g} \rightarrow {}^1E_u$
L_3	43.00	45.1	−1.3	*f*	*f*	0.09	0.00	$^1A_{1g} \rightarrow {}^1E_u$
C_1	45.32	55.1	0.6	0.7	0.6	0.25	0.29	$^1A_{1g} \rightarrow {}^1E_u$
C_2	47.72	52.6	8.8	*f*	*f*	0.02	0.06	$^1A_{1g} \rightarrow {}^1E_u$
C_3	48.37	50.0	−0.4	−0.4	0.6	0.67	0.66	$^1A_{1g} \rightarrow {}^1E_u$
X_1	55.60	*g*	0.0	*g*	*g*	0.40	*g*	$^1A_{1g} \rightarrow {}^1E_u$
X_2	61.90	*g*	0.8	*g*	*g*	0.50	*g*	$^1A_{1g} \rightarrow {}^1E_u$

[a] Observed values obtained as described in section IV. The magnitudes of the values for L and C bands may not be reliable although the signs are probably correct. [b] Contribution to the calculated value $\mathcal{A}_1^z/\mathcal{D}_0^z$ from the first (diagonal) sum of eq 19 by using Table III and CI coefficients of HRS.[9] [c] Sum of the absolute contributions to the second (interference) term of eq 19 by using Table III and the CI coefficients of HRS.[9] See the discussion of section IV. [d] $\mathcal{D}_0^z(Q)$ is the dipole strength of the entire Q-band region. [e] The oscillator strength (*f*) of HRS[9] is related to $\mathcal{D}_0$ by $\mathcal{D}_0 = 7.09 \times 10^5 f/\bar{\nu}$; see ref 7, p 540. [f] Wave functions for these transitions were not listed in ref 9. [g] HRS[9] did not calculate transitions above ~55 000 cm^{-1}.

TABLE V: Fitting Parameters for UV and Vacuum-UV Bands[a]

band	absorption $\mathcal{E}/10^3$ cm^{-1}	absorption Δ^b/cm^{-1}	absorption $\mathcal{D}_0/10^{-4}$	MCD Δ^b/cm^{-1}	MCD $\mathcal{A}_1/10^{-4}$	MCD $\mathcal{B}_0/10^{-8}$ cm
B_1	30.20	2567	1.39	2021	5.96	−1.61
B_2	29.95	372	0.05	578	0.17	−1.15
$N_1(0,0)$	35.61	485	0.23	485	0.26	−4.52
$N_1(1,0)$	36.19	525	0.09	525	0.11	−0.33
$N_1(2,0)$	37.02	484	0.06	484	0.05	1.25
N_2	37.92	749	0.06	749	−0.08	−1.14
L_1	39.40	423	0.04	1368	0.03	−6.82
L_2	41.10	1157	0.33	623	0.12	1.90
L_3	42.98	1267	0.33	923	−0.42	2.94
C_1	45.32	1480	0.89	887	0.49	−2.49
C_2	47.72	1029	0.06	1043	0.57	−3.00
C_3	48.37	2721	2.40	2865	−0.87	−8.87
X_1	55.60	3078	1.40	3078	−0.05	3.47
X_2	61.90	4000	1.75	4000	1.36	1.57

[a] All bands fit by using a Gaussian line shape and arbitrarily setting concentration times path length to unity. Intensity parameters $\mathcal{A}_1$, $\mathcal{B}_0$, $\mathcal{D}_0$ pertain to the fitted curves (dashed lines) of Figures 8–10, and the parameters for the B-bands are not normalized to the same scale as the others. However, direct comparison can be made by using the observed $\mathcal{D}_0^z$ ratios listed in Table IV. [b] Δ is the half-width at $1/e$ of maximum.

magnitude $|-4iC_1C_2\langle 2a_{1u}|l_z|4a_{2u}\rangle| \sim 1.7$. Thus the magnitude of our experimental value, $\mathcal{A}_1/\mathcal{D}_0 = 4.2$, can easily be rationalized if the cross term augments the diagonal term. These numbers lend support to our assumption that the ZnPc molecules are strongly oriented, since the maximum calculated value for the randomly oriented case is (eq 11a) $\bar{\mathcal{A}}_1(Q)/\bar{\mathcal{D}}_0(Q) = 2.1$, considerably below the observed value.

We have already shown that Q(1,0) consists of several overlapping vibronic overtones of Q(0,0) but that Q(2,0) contains a substantial contribution from a different electronic transition, Q′ (section V.1). Huang et al.[6] have demonstrated that Q′ corresponds to a transition to a singlet excited state and suggest that it arises from $e_u(N_{p_\sigma}) \rightarrow 6e_g(\pi^*)$ assisted by vibronic borrowing from Q(0,0) via e_g modes. This assignment is consistent with our experimental observations. Although the transition $^1A_{1g} \rightarrow {}^1A_{2u}^{Q'}$ is *z*-polarized, $^1A_{1g} \rightarrow {}^1A_{2u}^{Q'} \otimes e_g$ is *x*,*y*-polarized, and hence the observation of Q′ does not contradict our assumption of a highly oriented sample. In addition, a transition $^1A_{1g} \rightarrow {}^1A_{2u}^{Q'}$ should show only $\mathcal{B}$ terms in the MCD, as is observed. HRS calculate three transitions that are essentially $2e_u(N_{p_\sigma}) \rightarrow 6e_g(\pi^*)$, at 22 000, 31 400, and 42 300 cm^{-1}. The first of these lies closest to the observed energy ($\bar{E}(Q') = 16\,780$ cm^{-1}) but for the case of ZnPc corresponds to a transition terminating in a triplet excited state. We believe that the correct assignment is to the second of these calculated transitions and suspect that the energy of the $2e_u$ orbital in Figure 11 is too low.

As stated in section V.2, our observations in the B-band region are entirely consistent with the HRS prediction of two allowed $\pi \rightarrow \pi^*$ and one allowed $n \rightarrow \pi^*$ transition. Examination of the HRS wave functions shows that the states in this region involve strong CI among several excitations, the two most important being $4a_{2u} \rightarrow 6e_g$ and $3b_{2u} \rightarrow 6e_g$ with respective contributions of about 32% and 30% in the first and 37% and 25% in the second $\pi \rightarrow \pi^*$ transition. According to eq 18, in the absence of CI these two excitations give $\mathcal{A}_1/\mathcal{D}_0$ values of precisely the same magnitude but of opposite sign. Using the ω technique (Table III), we calculate, for example, $\mathcal{A}_1^z/\mathcal{D}_0^z = \pm 2.70$ respectively and thus might expect $\mathcal{A}$ terms of opposite sign. Inclusion of CI, however, changes the situation profoundly. Considering initially just the first (diagonal) terms on the right-hand side of eq 19, we note that the contributions of the two principal excitations ($4a_{2u} \rightarrow 6e_g$, $3b_{2u} \rightarrow 6e_g$) *almost cancel*, and thus $\mathcal{A}_1^z/\mathcal{D}_0^z$ *is determined primarily by the much less important excitations* (HRS[9] list coefficients for $2a_{1u} \rightarrow 6e_g$, $3a_{2u} \rightarrow 6e_g$, $5e_g \rightarrow 3b_{1u}$). Using these coefficients, one finds (Table IV) that *both* band B_1 and B_2 are predicted to have positive $\mathcal{A}_1^z/\mathcal{D}_0^z$ (0.4 and 0.5, respectively). In addition, because of the cancellation mentioned above, the second (interference) terms on the right hand side of eq 19 are especially important. Again using the HRS CI coefficients, we find (Table IV) the maximum *magnitude* of these contributions to $\mathcal{A}_1^z/\mathcal{D}_0^z$ to be 1.3 in both cases. (Recall that HRS do not give enough phase information to permit the *signs* of the interference terms

to be determined.) Certainly the large positive $\mathcal{A}_1^z/\mathcal{D}_0^z$ deduced for both bands B_1 and B_2 (Table IV) strongly suggests that the net interference term contribution is positive in both cases. But we note that the *maximum* calculated value (from Table IV) for $\mathcal{A}_1^z/\mathcal{D}_0^z$ can only be ~ 2 for both bands, which is only about half the experimental values. This discrepancy with experiment plus the lack of phase information and only a partial listing of the CI coefficients in the HRS calculation emphasizes the compelling need for a contemporary quantum calculation involving extensive CI.

Given the assignment for Q′ above, it is compelling to assign the z-polarized B_3 band to the transition $^1A_{1g} \rightarrow {}^1A_{2u}^{B_3}$ (principally $2e_u \rightarrow 6e_g$) calculated to lie at 42 300 cm^{-1}. As for the case of Q′, the observed energy of B_3 (32 200 cm^{-1}) lies more than 10 000 cm^{-1} below the calculated energy, which again suggests that the energy of the $2e_u$ MO in Figure 11 is too low.

HRS predict a number of weak transitions in the N-band and L-band regions but give explicit wave functions for only some of these. The strongest of the HRS transitions in the N-band region is calculated to lie at 38 300 cm^{-1}. The listed wave function for this transition shows CI to be very important but accounts for only 67% of the excited state. From this rather incomplete information we determine a diagonal contribution to $\mathcal{A}_1^z/\mathcal{D}_0^z$ of ~ 0.7 and an interference contribution of $|-4iC_1C_2\langle 1a_{1u}|l_z|3a_{2u}\rangle| \sim 0.0$ (Table IV). The resultant calculated value, $\mathcal{A}_1^z/\mathcal{D}_0^z \sim 0.7$, is in reasonable agreement with the observed value for N_1, $\mathcal{A}_1^z(N_1)/\mathcal{D}_0^z(N1) = 1.1$. The second of the observed N-band transitions, N_2, shows a negative $\mathcal{A}$ term and is weaker and at higher energy than N_1. On the basis of these three comparisons we have assigned N_1 and N_2 to the HRS transitions at 38 300 and 40 100 cm^{-1}, respectively.

In the L-band region, HRS predict one fairly strong band, at 47 700 cm^{-1}. This transition is dominated by the excitations $1a_{1u} \rightarrow 6e_g$ (36%) and $2b_{1u} \rightarrow 6e_g$ (17%), which give rise to opposing contributions to the MCD $\mathcal{A}$ term (eq 18). The cross term, $\langle 1a_{1u}|l_z|2b_{1u}\rangle$, is zero by symmetry, and so a weak positive $\mathcal{A}$ term is suggested. The listed wave function is incomplete (only 57% of the excited state is accounted for), but we obtain $\mathcal{A}_1^z/\mathcal{D}_0^z \sim 0.5$. Of the three transitions observed in the L-band region, L_2 agrees most closely with this value, $\mathcal{A}_1^z(L_2)/\mathcal{D}_0^z(L_2) = 0.4$, and is the most intense transition of the region. Thus we assign L_2 to the transition that HRS calculate at 47 700 cm^{-1}. There is insufficient information to convincingly assign the remaining transitions, but on the basis of their relative energies we have chosen to assign L_1 and L_3, respectively, to the transitions that HRS calculate at 42 900 and 45 100 cm^{-1}.

HRS calculate several relatively intense transitions in the C-band region. The most intense, at 50 000 cm^{-1}, is listed as having a major contribution (41%) from $2a_{1u} \rightarrow 7e_g$ and is the first transition in which excitation to $7e_g$ is dominant. According to Table III and eq 18, the $2a_{1u} \rightarrow 7e_g$ excitation will make a negative contribution to $\mathcal{A}_1/\mathcal{D}_0$. However, CI is very important for this excited state, and some of the other excitations give rise to opposing contributions. The CI coefficients listed by HRS account for only 69% of the excited state, but using these and the matrix elements of Table III, we calculate a total diagonal contribution to $\mathcal{A}_1^z/\mathcal{D}_0^z$ of -0.4 and an absolute interference contribution of $|-4iC_1C_2\langle 2a_{1u}|l_z|4a_{2u}\rangle| \sim 0.6$. Thus the $\mathcal{A}$ term associated with this transition may be quite weak but is probably negative. The only negative $\mathcal{A}$ term that is observed in the C-band region is associated with C_3. Although C_3 is not the lowest energy transition observed in the C-band spectrum, it is the most intense, and hence we assign it to the HRS band at 50 000 cm^{-1}. The only other transition for which HRS explicitly list a wave function is the second most intense of the region and occurs at 55 100 cm^{-1}. The corresponding excited state shows a high degree of configuration mixing. The listed wave function accounts for only 57% of the total but gives a diagonal contribution to $\mathcal{A}_1^z/\mathcal{D}_0^z$ of ~ 0.7 and an interference contribution of ~ 0.6. On the basis of the sign of the $\mathcal{A}$ term and the intensity of the absorption, we assign C_1 to this transition. The remaining band observed in the C-band region, C_2, has been tentatively assigned to the 52 600-cm^{-1} transitions of HRS, although there is really insufficient information to discriminate between this transition and the one at 43 900 cm^{-1}.

The analysis presented above is rather subjective in several regards. HRS do not give wave functions for all of the transitions that they calculate, and where they do, the listed wave functions are incomplete. The observed parameters for the higher energy transitions (the L-band and C-band regions in particular) are obtained by fitting strongly overlapping bands and may not be quantitatively reliable. Despite these problems we believe that the correlations we draw are reasonable in the context of the available results, and we are encouraged by several aspects of the comparison presented in Table IV. First, we observe nearly all of the $\pi \rightarrow \pi^*$ and $n \rightarrow \pi^*$ transitions calculated by HRS within the region that they considered. Second, the general distribution of observed transition intensity among the various regions of the absorption spectrum is in reasonable accord with the calculations (Figure 2 and Table IV). Third, in each region we find transitions that exhibit the same MCD dispersion forms ($\mathcal{A}$ or $\mathcal{B}$ terms), the same signs, and in the case of $\pi \rightarrow \pi^*$ transitions, roughly the same $\mathcal{A}_1/\mathcal{D}_0$ ratios as predicted by the HRS calculation and the matrix elements of Table III. The results and comparisons presented here should provide a basis for a contemporary quantum calculation of the excited states of the Pc ring. The angular momentum information provided by the MCD data in particular should provide a stringent test of excited-state wave functions.

VII. Comparison with the Analysis of Nyokong, Gasyna, and Stillman (NGS)[1]

We here compare our results and analysis with the recent study of ZnPc in solutions, complexed with CN^-, imidazole (Im), and pyridine.

In the Q-band region, our data are far better resolved, presumably because of the lower temperature and the isolation of our sample in a matrix. We see three distinct envelopes labeled Q(0,0), Q(1,0), and Q(2,0) (Figures 5–7). NGS clearly see the Q(0,0) band and its associated positive $\mathcal{A}$ term, but they deconvolute the sidebands into five components, each with an associated $\mathcal{B}$ term. It is clear from section V.1 that these sidebands arise from numerous overlapping vibronic bands and a separate electronic transition. The deconvolution of NGS probably reflects this complexity.

NGS report $\bar{\mathcal{A}}_1(Q)/\bar{\mathcal{D}}_0(Q) = 1.67$ and 0.73 respectively for $ZnPc(CN^-)$ and ZnPc(Im). Assuming that our sample is completely oriented (section IV.2), we multiply the NGS values by 2 for comparison with $\mathcal{A}_1^z(Q)/\mathcal{D}_0^z(Q)$ for ZnPc/Ar. In that case the values of NGS are lower than our value ($\mathcal{A}_1^z(Q)/\mathcal{D}_0^z(Q) = 4.2$), particularly for the case with Im. Similar discrepancies are found in the B-band region, where NGS find $\bar{\mathcal{A}}_1(B)/\bar{\mathcal{D}}_0(B) \sim 1.0$ and ~ 1.4 respectively for CN^- and Im, compared with our value of $\mathcal{A}_1^z(B)/\mathcal{D}_0^z(B) \sim 4.4$. It would appear that interaction with axial ligands in solution significantly lowers the excited-state orbital angular momentum in the Pc ring. Such effects have been observed previously for the case of axially ligated metalloporphyrins.[24] For example, in the case of the Zn complex of porphine, the value of $\mathcal{A}_1/\mathcal{D}_0$ for Q(0,0) is reduced by more than 50% on coordination of an axial pyridine ligand and actually changes sign with coordination of CN^-. The reduction of $\mathcal{A}_1/\mathcal{D}_0$ has been interpreted as arising from structural and/or vibronic effects.[24]

NGS reassign the traditional location of the B, N, and L bands by correlating each distinct $\mathcal{A}$ term in their MCD spectra with a single MO excitation. Specifically (Figure 1 in ref 1), their correlations (translated into our MO numbering scheme) and energies[1] are $2a_{1u} \rightarrow 6e_g$ (Q band, 14 900 cm^{-1}), $4a_{2u} \rightarrow 6e_g$ (B band, 27 500 cm^{-1}), $1a_{1u} \rightarrow 6e_g$ (N band, 29 800 cm^{-1}), $2a_{1u} \rightarrow 7e_g$ (L band, 35 400 cm^{-1}), and C band (40 600 cm^{-1}). While in one sense this is a notational matter, such a scheme can be subject to serious misinterpretation, since it seems to imply that each MO excitation can be associated with a specific spectroscopic transition

(24) Keegan, J. D.; Bunnenberg, E.; Djerassi, C. *Spectrochim. Acta* **1984**, *40A*, 287–297.

of the system. Examining the calculation of HRS (Table 4 in ref 9) as an illustration, we note that this is in fact only (roughly) true for the Q band, where the $2a_{1u} \rightarrow 6e_g$ excitation makes a contribution of ~80%. In the B-band region, the $4a_{2u} \rightarrow 6e_g$ excitation contributes only ~35% to the spectroscopic transition while $3b_{2u} \rightarrow 6e_g$, for example, makes a contribution of a similar magnitude. In this same vein, the HRS calculation indicates that the $1a_{1u} \rightarrow 6e_g$ excitation makes a negligible contribution in the region of 30 000 cm^{-1} so there is no basis at all for assigning[1] the $\mathcal{A}$ term at 29 800 cm^{-1} in ZnPc (Im) to this excitation. In fact, in earlier work on MPc films, Hollebone and Stillman[25] suggested the same basic interpretation for the two $\mathcal{A}$ terms in the (traditional) B-band region that we adopt in the present work (see particularly p 2123 in ref 25). In general, configuration interaction plays an increasingly important role as we move to higher energy.

We would strongly urge that the traditional meaning of the Q, B, N, L, C, and X nomenclature be retained (Figure 2), with the understanding that each of these regions may contain several transitions.

VIII. Vacuum-Ultraviolet Transitions

In an earlier note[10] we reported the vacuum ultraviolet MCD and absorption spectra of ZnPc/Ar, which our present work shows to be largely erroneous. Most of the intensity in the L-band and C-band regions of the earlier data can now be attributed to the presence of phthalonitrile (Pn), a starting material in the preparation of Pc's (see section II). The bands labeled C_b–C_e are almost exclusively due to Pn, a fact we confirmed by making comparisons with the spectra of pure Pn in an Ar matrix.[11] In addition the feature at ~48 200 cm^{-1}, which we had earlier denoted C_a and had attributed to localized transitions of the fused benzene rings of the Pc ligand,[10] is due to a $^1S \rightarrow {}^1P$ transition of atomic Zn.

The progression of sharp bands observed between 62 500 and 76 900 cm^{-1}, which was previously assigned as the X_2 band and characterized as a Rydberg transition,[10] can be entirely eliminated from the ZnPc/Ar spectrum. We have shown this by studying the rate of growth of spectral features with deposition rate and temperature. The bands shown in Figure 10 grow in unison, but the sharp progression referred to above begins to appear only at elevated sublimation temperatures.

Despite the earlier misassignments in the vacuum-UV,[10] we still feel that some of the transitions in the vacuum-UV involve excitations to Rydberg states. For example, the X_2 band is considerably sharper in the gas-phase absorption spectrum than in condensed-phase (matrix and thin-film) spectra and appears to show a slight blue shift on condensation (Figure 2). This type of behavior is that which we would expect for a Rydberg transition. Again we suggest that there is a need for a contemporary quantum calculation, and it would be desirable if such a calculation could utilize a sufficiently large basis set to allow for the possibility of Rydberg transitions.

IX. Conclusion

We have presented absorption and MCD data for ZnPc isolated in an Ar matrix over a very wide energy range, ~14 300–74 000 cm^{-1}. The use of matrix isolation and its accompanying low temperature affords us well-defined spectra over the entire region. We are able to characterize the energies and angular momenta of many excited states and generally find them in qualitative accord with the calculations of HRS.[9]

There is clearly a need for a contemporary quantum calculation of the Pc ring system, and the angular momentum information provided by the MCD data in particular should provide a stringent test of excited-state wave functions, particularly in the high-energy region where configuration interaction (and perhaps Rydberg states) become very important. It is encouraging that reasonable correlations can be drawn with an older quantum mechanical calculation,[9] which permits rationalization of many spectroscopic features. What is sorely needed are explicit wave functions to permit the calculation of angular momentum matrix elements.

In future work we will present matrix isolation MCD data on other MPc systems (M = open-shell transition metals or lanthanides) as well as on the Zn complex with tetrabenzoporphyrin. The latter permits an interesting comparison of the effects of substituting the aza N atoms in the Pc ring by C atoms.

Acknowledgment. We gratefully acknowledge the assistance of the staff of the Synchrotron Radiation Center, University of Wisconsin—Madison. We especially thank Dr. P. A. Snyder for the use of some of her equipment. We thank Dr. B. I. Swanson for illuminating comments on the orientation of Pc's in matrices and Professor M. J. Stillman for the sample of ZnPc. A.E.S. thanks the Deutsche Forschungsgemeinschaft, Federal Republic of Germany, for the award of a postdoctoral fellowship. P.N.S. thanks Dr. Peter Day, the Fellows of St. John's College, and the Inorganic Chemistry Laboratory, Oxford University, for their generous hospitality while part of this work was carried out. This work was supported by the National Science Foundation under Grants CHE8400423 and CHE8700754.

Registry No. ZnPc, 14320-04-8; Ar, 7440-37-1.

(25) Hollebone, B. R.; Stillman, M. J. *J. Chem. Soc., Faraday Trans. 2* **1977**, *74*, 2107–2127.